APPLICATION OF HYPERSPECTRAL REMOTE SENSING IN DETECTING AND MAPPING SERICEA LESPEDEZA IN MISSOURI

A Thesis
Presented to
The Faculty of the Graduate School
University of Missouri-Columbia

In Partial Fulfillment
Of the Requirements for the Degree

Master of Arts

---

by

BO ZHOU

Dr. Cuizhen Wang, Thesis Supervisor

May 2007

The undersigned, appointed by the dean of the Graduate School, have examined the thesis entitled

APPLICATION OF HYPERSPECTRAL REMOTE SENSING IN DETECTING AND MAPPING SERICEA LESPEDEZA IN MISSOURI

presented by Bo Zhou

a candidate for the degree of Master of Arts

and hereby certify that in their opinion it is worthy of acceptance.

_____

Cuizhen Wang
Assistant Professor
Department of Geography

_____

C. Mark Cowell
Associate Professor
Department of Geography

_____

R. David Larsen
Associate Professor
Department of Forestry

Acknowledgements

It is a great accomplishment for me to finish this research. I am very proud of myself. But deep in my heart, I am extremely grateful for those who have helped me all the way to this point for whom I can not do without. To mention everyone who helped me will take up a substantial space. My parents are the ones to be thanked in the first place for making me who I am and for supporting me to do what I want. I will always be grateful to their unconditional and overwhelming love. My parents are the ones who supported my ideas and my dreams.

Professor Susan Wang, my advisor, is the person who makes everything possible for me. Before I came to the United States, I had some initial contact with Dr. Wang who showed great interests in my research experience and tried very hard to bring me here for my Master's study. Dr. Wang also helped me tremendously when I first came here who was able to make life easier for me as it should be for a new comer to a completely new environment and society. It is a great experience to work with Dr. Wang as her TA through which I learned tremendous knowledge and experience that could be applied to my future research. Dr. Wang is always available when I need her help and she is so approachable as teacher, so resourceful as a mentor and so considerate as a person. I still remember vividly last year when we were both out into the fields collecting ground data and explore the possibility of using hyperspectral imagery to detect weeds. Whenever I encountered any problem that stopped me from progressing in my research, she was able to figure out a way that drag me out of trouble and put me on the right track. Overall, Dr.

Wang is the single most important reason that I was able to accomplish anything in my research. I am extremely grateful to her help in all sorts of ways.

I would also like to thank my committee members, Dr. Mark Cowell and Dr. David Larsen, who unconditionally agreed to be on my committee and gave me great support with suggestions together with their perspectives toward my research. I am grateful to their valuable time and patience toward a Master's student like me.

I should also direct my thanks to Dr. Harlan Palm for organizing to acquire the image that is used in this research. Without the image my research could have never been done. Dr. Palm is the person who brought in the issue of sericea invasion as the start point of my thesis study. He also guided Dr. Wang in locating feasible study areas in Mid-Missouri. Besides Dr. Palm, Ms. Becky Erickson in the Regional Office of Missouri Department of Conservation (MDC) should also be given huge credits to for spending a whole day showing us fields invaded by sericea. She was the person who showed us the study area that we later picked in my research. I really admire her professionalism and her devotion to her work and her passion to share her knowledge with us without asking any reward.

I will also thank the Geography department of University of Missouri-Columbia for supporting me my TAship for my Master's study, for giving me the opportunity to study and research in a good environment without having to worry about how to survive, and for sponsoring me my field work during last summer. I would also like to thank the Graduate Professional Council (GPC) of University of Missouri-Columbia for supporting

my travel to the 2007 Annual meeting of the Association of American Geographers (AAG) in San Francisco, CA. to present my research and broadcast my findings in the effort to control weeds in the state of Missouri. Finally, I would like to thank the Geography Resource Center (GRC) of Geography department for allowing me accessing the ENVI software in my research.

TABLE OF CONTENTS

LIST OF FIGURES

FIGURE PAGE

LIST OF TABLES

ABSTRACT

APPLICATION OF HYPERSPECTRAL REMOTE SENSING IN DETECTING AND MAPPING SERICEA LESPEDEZA IN MISSOURI

When conservationists in Missouri realized that sericea lespedeza was taking its toll by threatening the healthy growth of economic vegetation, they decided to start controlling the invasion of this species. A major challenge encountered is to map the extent of its spatial spread. While satellite remote sensing and aerial photography have been available for many years, newer detection technologies such as hyperspectral sensors have made it possible to acquire large-scale laboratory-like spectra of sericea patches and surrounding natural grasses in the air. In this study, sericea was mapped using the Airborne Imaging Spectrometer for Application (AISA) sensor that records images at high spectral (9nm bandwidth, visible-infrared) and spatial (~1m) resolution. Ground spectra were measured using the FieldSpecPro Full Range (FR) spectroradiometer from Analytical Spectral Devices (ASD, 2006). The study area is a grass field within the Mark Twain National Forest. The AISA images were processed with three different classification methods, and the results are validated based on field surveys. Major findings include: (1) the averaged sericea spectra is more accurate for mapping purposes; (2) moderate spectral response instead of strong spectral response is better in sericea mapping for they have less confusion with other classes; and (3) the MNF (Minimum Noise Fraction) and MTMF (Mixture Tuned Matched Filtering) approach is the best for mapping sericea.

Key words: Hyperspectral remote sensing, weed invasion, classification.

CHAPTER 1
INTRODUCTION

Plant invasions are a current threat to biodiversity conservation, second only to habitat loss and fragmentation (Yates 2004). Plant invasions are usually caused by non-native species that are introduced to a native environment. All species on the Missouri noxious weed list are invasive plants; that is, they have been introduced into an environment in which they did not evolve and often have no natural enemies to limit their reproduction or spread (Fishel 2002). Of the more than 2,500 plant species in Missouri, about 25 percent are considered as nonnative and are called noxious weeds (Fishel 2002).

There are several reasons that these non-natives are a threat to the native ecosystem. First, they are superior competitors in disturbed environments, and will contend for light, water, nutrients and space (Fishel 2002). Second, noxious weed species interfere with agriculture, cause human health problems, and degrade the environment (Fishel 2002). Finally and most importantly, noxious weeds reduce land value (Fishel 2002). As a result, they need to be controlled or eliminated based on their threat level to the native ecosystem. Herbicides are sometimes used to fulfill this task. Herbicides make up the vast majority of pesticide inputs to Missouri agronomic productions. The Missouri Department of Agriculture estimates that corn produced in 1999 applied about 97 percent of their pesticide inputs, by weight, in herbicides (Fishel 2002). To improve the efficiency of herbicide application, it is better through mapping the distribution of noxious weeds

and then spraying only on areas with the existence of noxious weeds. Weeds often cluster in patches. Several physical and chemical soil properties, such as pH, nutrient levels, organic matter content, and cation exchange capacity are believed to contribute to "patchy" weed distributions (Koger 2003). This patchy pattern could be detected with remotely sensed images. In this research, a specific noxious weed type commonly named sericea lespedeza with a scientific name of *Lespedeza cuneata L.* (USDA plants database 2007) hereafter referred to as sericea, is mapped in grass fields in Mid-Missouri using an airborne image.

1.1 Sericea

Sericea is recognized as "Missouri's silent thief" (Bové 2004). In pastures, sericea has been found to have allelopathic qualities that hinder germination or growth of both warm and cool season grasses typical of pastures (Dudley 2003). Though it was not officially categorized as an invasive species in Missouri until most recently, the damage is already present in a large portion of this state (Bové 2004).

1.1.1 What is sericea

Sericea is a warm-season, perennial legume native to eastern Asia (Figure 1-1). It was intentionally introduced into the United States in the late 1890s (Brush 2001). Sericea is a deep-rooted perennial that can grow 18 to 40 inches tall. Stems are either single or clustered with many branches. Mature stems are coarse or woody in appearance. Leaves are a trifoliate with short petioles. Flowering occurs from mid-July to early August (Brush 2001).

Figure 1-1: A tract of pasture land dominated by sericea (Cedar Creek Ranger District, Mark Twain National forest, Missouri. photographed by Bo Zhou, July 2006)

1.1.2 Sericea invasion

Sericea was first introduced to Missouri by the Missouri Department of Transportation (MoDOT) to control highway road-side erosion in the 1930s (Brush 2001; Bové 2004). It was later found by the Missouri Department of Conservation (MDC) that sericea's disadvantages far outweigh any possible benefits due to several innate features of this plant (Bové 2004). Sericea succeeded in creeping across the fence into fields of pasture or hay ground (Brush 2001). Once you know what to look for, you're sure to spot it everywhere you go in Missouri, especially along roads (Bové 2004). Because of its highly competitive nature, poor forage quality and invasiveness, sericea was put on Kansas's noxious weed list in July 2000. It was not put on the noxious weed list in

Missouri until 2004 (Bové 2004), due to the fact that too much sericea has been sown for erosion control, and there are some areas in the state where seed is grown and harvested and sold for use in other states (Brush 2001).

Land managers with MDC currently scout statewide conservation land for sericea and the Missouri Prairie Foundation has been spraying herbicide on sericea in its land as well on selected MDC lands. But due to the persistence of this species, people sometimes attempt to control it by burning the fields (Bové 2004).

1.2 Remote Sensing

1.2.1 Current situation

Remote sensing is the science and art of obtaining information about the properties of electromagnetic waves emitted, reflected or diffracted without touching the object (Campbell 2002). Remote sensing provides a unique perspective in mapping and monitoring large areas because it measures emitted or reflected energy at wavelengths with a wider range than human vision (e.g., infrared, microwave, etc.).

Remote sensing is widely explored as a tool for detection and mapping of weeds in agricultural crops (Lamb and Brown 2001). Remote sensing-based approaches have been developed for operational monitoring of weed invasion (Thorp and Tian 2004). Weeds often cluster together to form “patchy” effects that could be identified using remotely sensed images (Thorp and Tian 2004). In past studies classification algorithms were often applied to delineate weed patches based on statistical variability in the different spectral response of vegetation and non-vegetation canopies. However, for post-emergence weed

sensing, the effectiveness of classification is weakened since weeds and crops exhibit similar spectral characteristics (Lamb and Brown, 2001).

1.2.2 Sensor limitations

Application of multi-spectral remote sensing in weed detection is limited because of its spectral configuration and sometimes low spatial resolution. The low spatial resolution of satellite image such as Landsat Thematic Mapper (TM) is not feasible for weed detection since there may be too much confusion inside a pixel. The spectral response of a single pixel is often a mixture among several targets (Thorp and Tian 2004). Airborne photos or satellite images with high spatial resolution (e.g., IKONOS, QuickBird), on the other hand, have problems with the lack of a sufficient number of narrow spectral bands to detect minor differences between different type of vegetation. Still other sensors with high spectral resolution like Moderate Resolution Imaging Spectroradiometer (MODIS) are not capable of weed detection because of their low spatial resolution.

The problem with most widely used multispectral systems is that they only have a limited number of bands with each covering a very wide region in the spectrum (> 100nm). Within such a wide spectral region a lot of subtle information is averaged, generalized or even concealed. Figure 1-2 shows how the information is lost by using multispectral RS. Unique spectral features of a weed species, such as reflectance peaks or absorption troughs in the spectrum, are often lost in broad-band spectral reflectance.

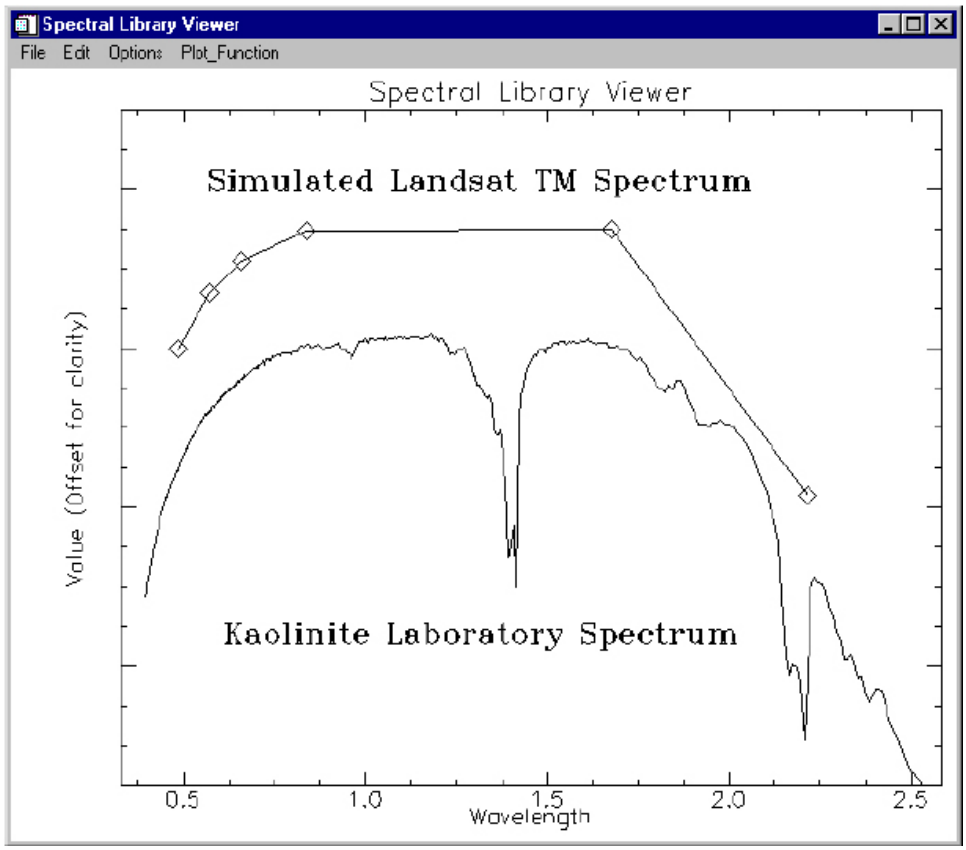

Figure 1-2: Spectrum comparison between Multi- and Hyper-spectral signatures (ENVI 2002)

1.2.3 Hyperspectral substitution

Hyperspectral sensors can capture data in contiguous, narrow bands in the electromagnetic spectrum. The large numbers of bands provide researchers with vast quantities of information (Goetz 1985). Hyperspectral data can often capture the unique spectra or 'spectral signature' of an object. This signature can be used to differentiate and identify materials (Goetz 1985).

Hyperspectral remote sensing integrates imaging and spectroscopy in a single system which often includes large data sets due to the fine narrow subdivision of bands and the "hyper" number of bands in the spectrum. A "band" is defined as a portion of the

spectrum with a narrow spectral width such as 10nm. Hyperspectral remote sensing records more detailed spectral information for weed detection and other applications of target identification. However, the large size of data set takes up more storage space and requires new and more complicated processing algorithms (Goetz et al. 1985).

Different ground objects tend to have different 'spectral signatures' corresponding to their identity. In this study, hyperspectral imagery is used to detect and map sericea based on its unique spectral response. Figure 1-3 and 1-4 show the side and top views of sericea. Also note the patchy effect of sericea in Figure 1-3.

Figure 1-3: Side-view of sericea (Cedar Creek Ranger District, Mark Twain National forest, Missouri. photographed by Bo Zhou, July 2006)

Figure 1-4: Close-up view of sericea from above (Cedar Creek Ranger District, Mark Twain National forest, Missouri. photographed by Bo Zhou, July 2006)

Good results from hyperspectral analysis are possible in this study because it is suggested that hyper-spectral RS might be more successful for weed species delineation than multi-spectral RS (Varner 2000).

1.3 Research objective

Sericea encroachment has been serious in Missouri. Although it was introduced and treated as a boon for wildlife and erosion control, it is now the subject of eradication efforts (Bové 2004). Before conservationists can start removal of these noxious weeds, they will first need a distribution map to guide the task. Although field surveys are accurate, they are very time consuming and accessibility is an issue because huge parts of

Missouri pastures are private lands. A newer and more effective approach is called for. In this research the feasibility of hyperspectral remote sensing for mapping sericea in Missouri will be tested. To fulfill this goal, several research objectives will be accomplished:

(1) Select optimal bands in hyperspectral images that are most useful in classification,

(2) Identify optimal endmember, signature spectrum that represents a certain class, for sericea classification, and

(3) Test effective classification algorithms to accurately map sericea.

CHAPTER 2

LITERATURE REVIEW

2.1 Multispectral remote sensing in agriculture

2.1.1 Crop mapping

Agricultural fields during the growing season have distinctly different color, pattern and texture from other land cover types such as forest and water. As a result, large-area crop mapping can be easily conducted from multispectral images at medium to coarse resolution. More detailed information can be extracted from multispectral images at high resolution to meet the requirements of site-specific farming (Barnes 1996).

Perhaps the most widely accepted method for image-based crop monitoring is to extract greenness and healthiness information by calculating band ratios or vegetation indices (Thorp and Tian 2004). Vegetation indices can be used to estimate soil properties such as organic matter (Dalal and Henry 1986; Shonk et al. 1991). Vegetation indices are also used for water stress detection (Barnes 1996). Many of these indices have been developed for use in remote sensing research over the past 30 years. Among them the most widely used one is the normalized difference vegetation index (NDVI; Ashley and Rea 1975). In addition to the NDVI, the other two most basic vegetation indices (VI) are ratio vegetation index (RVI; Jordan 1969) and difference vegetation index (DVI; Tucker 1979). These basic vegetation indices can easily separate vegetation spectra from other

spectra such as soil and water. However, they are highly affected by soil background and other geometric/systematic factors. Several more advanced VIs are introduced such as Soil Adjusted Vegetation Index (SAVI; Huete 1988) and a similar Transformed Soil Adjusted Vegetation Index (TSAVI; Baret 1989) that reduces soil effect in the calculated VIs. Later a more advanced Modified Soil Adjusted Vegetation Index (MSAVI; Qi 1994) is introduced to interactively adjust for soil effect in each area instead of using a constant soil factor value as in SAVI. Vegetation indices have always been widely applied in agricultural studies.

2.1.2 Invasive species detection

Because of the small size of invading weeds and the spectral similarity with crops in the fields, the application of multispectral remote sensing in weed detection has been limited. Fitzgerald (2000) examined the possibility of using multispectral remote sensing in detecting spider mite on cotton in California. He also tested the feasibility of early detection using multitemporal data. A lot of techniques were compared in his research, such as principal components analysis, classification and change detection. The implications of this research are bi-fold in that it tested the critical cut-off time of detecting invasive species and also looked at the trend of invasion by examining data in a series of time.

Low altitude and higher-resolution systems have potential to characterize weed texture (Smith 2003), but only after full growth when vegetation texture is formed. Although it is desirable to detect invasive species in early stage to allow corrective actions to be taken, multispectral remote sensing has limited capability of detecting infestation in very early

stages (Smith 2003). It might be more useful in late-season weed infestation detection. Koger (2003) found that late-season weed infection in soybean fields could reach an accuracy of over 90% with NDVI derived from multispectral image.

The primary limit in detecting weed invasion with multispectral remote sensing comes from its broad band settings that conceal a lot of minor variation inside the real continuous spectra. In previous research, it was found that some of the background effects could be substantially reduced using narrow-band derivative-based vegetation indices (Elvidge 1995). Therefore hyperspectral remote sensing is more desirable when subtle spectral variation is needed in agricultural studies.

2.2 Hyperspectral remote sensing in agriculture

2.2.1 Image Spectrometry

Image spectrometry, a new technique for remote sensing of the earth, is technically feasible from aircraft and spacecraft platform. The airborne and spaceborne sensors are capable of acquiring images simultaneously in 100 to 200 contiguous spectral bands depending on application necessity and system configuration. The ability to acquire laboratory-like spectra remotely is a major advance in remote sensing capability. It is now possible to remotely identify a surface material on a pixel basis by examining its absorption features in the continuous reflectance spectrum (Goetz 1985). An example of material identification is shown in the following Figure 2-1. The spectral resolution of the library spectra is 1 nm. All of the five materials are completely separable given good band selection and combination. If hyperspectral remote sensors can obtain images with

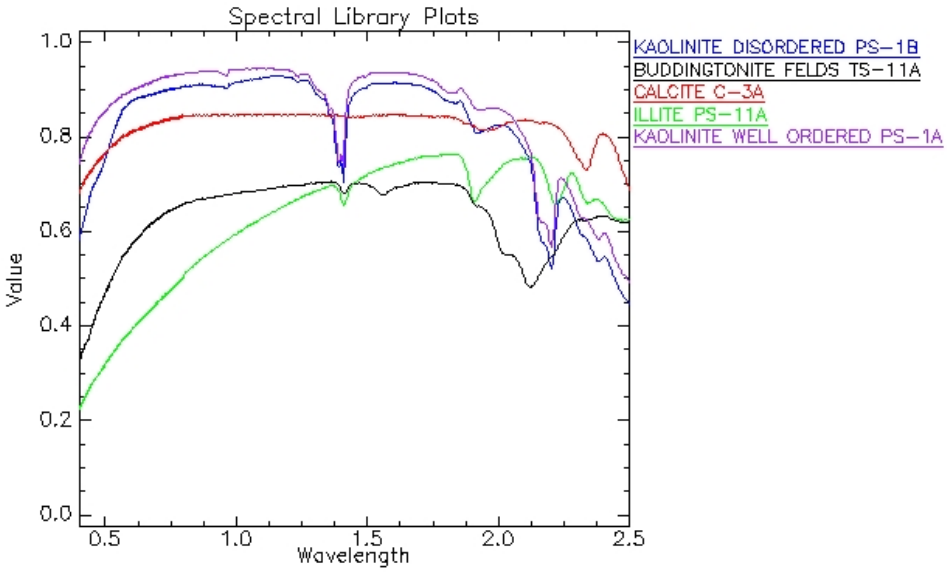

Figure 2-1: Sample spectral plot from JPL spectral library (ENVI 2002)

such high spectral resolution, the image could be directly referenced to the library spectra to perform material identification.

A considerable number of spaceborne or airborne spectroscopic devices with as many as 200 spectral bands are now flying in a number of countries. Despite the much narrower spectral bands being used, they can provide signal-to-noise ratios supporting 10-12 bit data systems with spatial resolutions of a few 10's of meters IFOV (Instantaneous Field Of View) from orbit and roughly 1 meter resolution for airborne sensors (Landgrebe 1993).

2.2.2 Invasive species detection

The most extensive hyperspectral remote sensing agricultural application is perhaps precision farming. In precision farming, scientists care most about the healthy growth of economic vegetation. Therefore they will need hyperspectral remote sensing as tool to

detect any phenomenon that is hampering the healthy growth of economic vegetation. Problems related to precision farming like malnutrition, pest invasion and weed infestation in a particular crop can be observed in a unique spectrum which is distinctly different from healthy vegetation (Gat, Erives, Maas and Fitzgerald 1999). Various approaches of hyperspectral data processing have been developed for invasive weed detection. For example, Garegani, et al. (2000) applied Minimum Noise Fraction (MNF) approach to detect stressed crops. Zhang (2003) used hyperspectral data to detect stress in tomatoes induced by late blight disease in California by using MNF rotated spectra as an input to Spectral Angle Mapper (SAM) classification. More well-rounded invasive species detection and mapping application was done by Ustin (2002) and Underwood (2003) in California's Mediterranean ecosystems. In their studies, several classification methods were investigated and compared: (1) continuum-removal, (2) MNF, (3) band ratios, and (4) SAM each with different justification and consideration. The first one was used to pick up the water absorption features in the spectrum, while the second approach took advantage of the information in full image spectrum and still able to reduce the dimensionality of the hyper-bands. The third method was selected on the basis that band ratio is very sensitive to biochemical and biophysical properties of vegetation, and the last approach took advantage of the dimension of the hyperspectral dataset to come up with an angle measurement plotted in the multi-dimensional space by each individual vegetation spectrum. The accuracy was very high although it varied over different test sites.

Other advanced approaches have been previously explored. Vrindts, et al. (2002)

developed a statistical approach toward invasive species detection. Fitzgerald (2004) applied the Spectral Mixture Analysis (SMA), also called linear un-mixing approach, to de-correlate each pixel into several basic components to enhance classification accuracy. The temporal consideration in hyperspectral remote sensing was also discussed by Dennison (2003) in which he found that there was a negative correlation between the increase of non-photosynthetic vegetation (NPV) and soil water balance decrease. He also reported that variation in water deficit image resulted in large confusion in classification. A larger number of endmembers were suggested to enhance the classification accuracy while the seasonal variation in the spectral response should be taken into account in vegetation classification. Among these studies the MNF or MNF combined approach yields very good result in crop mapping. The MNF approach is also utilized in this thesis research.

2.3 Hyperspectral data analysis

Hyperspectral data analysis can be divided into two categories (Aspinall 2002). One is top-down, which essentially uses field maps to train the imagery so as to detect certain features of the examined objects. Field survey and geo-referencing are necessary because high positioning accuracy is needed in this approach. Atmospheric correction of the imagery may not be needed in this approach. Since the high spatial resolution image usually does not have large extent coverage, the atmospheric variation within each scene is not noticeable. Associating the ground features directly with the image will enable the classifying algorithm to incorporate atmospheric effects into the feature spectra to search for similar features on the same image. This approach is not feasible for large physical

extent analysis (Aspinall 2002).

The other approach, in contrast, is bottom-up which typically uses ground- or lab-measured spectral libraries to identify features in the image. Atmospheric correction is essential because atmospheric effects have to be removed from the image before it can be quantitatively compared with ground-measured spectra (Kruse 1994). Geo-referencing and registration are necessary to match geographic positions of image pixels to ground sites. To reduce spectral noise, the absorption regions such as affected by water and carbon-dioxide of the spectrum should be removed before further processing.

2.3.1 Atmospheric correction

Removing atmospheric effect involves calibration and atmospheric correction. Calibration adjusts the image by converting raw radiance values of each pixel to top-of-atmosphere absolute (radiance) or relative (reflectance) values. Atmospheric correction then adjusts these values to ground radiance or reflectance at each pixel based on sun-ground-sensor geometry and atmospheric composition. In general the approaches of hyperspectral atmospheric correction could be divided into three categories: (1) Scene-Based Empirical Approaches, (2) Radiative Transfer Modeling Approaches, and (3) Hybrid Approaches (Gao 2006).

2.3.1.1 Scene-Based Empirical Approaches

During the mid-1980s, several scene-based empirical approaches were developed to remove atmospheric effects from hyperspectral image and to derive surface reflectance spectra. Among these methods, flat field calibration (Goetz and Srivastava 1985; Roberts

et al. 1986) and internal average relative reflectance (IARR; Kruse et al. 1985; Kruse 1988) could produce relative reflectance spectra. Flat field calibration utilized a known area of reflectance on the image, usually defined as a Region of Interest (ROI), to normalize the raw radiance. The radiance spectrum from this area is assumed to be resulted from pure atmospheric effects. It is then used as normalization factor to divide the raw spectra at each pixel of the image. The resultant ratio is the relative reflectance and could be compared with laboratory spectra. The IARR Calibration technique is used to normalize images with a scene average spectrum. This calibration method is performed by calculating an average spectrum from the entire scene which is used as a reference spectrum. The apparent reflectance is then calculated by dividing the reference spectrum with the pixel value. This technique is often used to convert imaging spectra to relative reflectance when ground spectral measurement is not available. It works best in arid areas with limited vegetation cover.

Empirical Line correction (Roberts et al. 1985; Conel et al. 1987; Kruse et al. 1990) can be used to calculate apparent (absolute) reflectance. The Empirical Line correction technique forces image spectra to match selected field reflectance spectra. This method requires ground measurements and/or knowledge of the environment (laboratory spectra). Two or more ground targets need to be identified and reflectance of each target is measured in the field or colleted from laboratory spectra. Usually the targets consist of at least one light and one dark area and then identified in the image scene. A linear regression is performed to calculate the gain and offset which are used to calculate reflectance at each band. This process is equal to removing the solar irradiance and the

atmospheric effect. The processed spectra are most comparable to field or laboratory spectra.

2.3.1.2 Radiative Transfer Modeling Approaches

Surface reflectance can also be derived from hyperspectral images using Radiative Transfer Functioning (RTF) approaches (Gao 2006). The Atmospheric Removal Program (ATREM; Gao and Goetz 1990; Gao et al. 1993) is a RTF-based calibration method to calculate absolute reflectance that requires no ground-based measurement. This method was first developed for airborne AVIRIS imagery that has 224 bands. It uses water absorption bands to calculate the amount of water vapor atop of each pixel. This information is then used to calculate surface reflectance in the Simulation of Satellite Signals in the Solar Spectrum (5S) model (Tanre 1990). Other RTF models such as MODerate resolution atmospheric TRANsmission (MODTRAN) can be used to in this process to calculate surface reflectance (Berk et al. 1998).

More atmospheric correction algorithms for retrieving surface reflectance include the Atmospheric CORrection Now (ACRON; Berk et al. 1999), and the Fast Line-of-sight Atmospheric Analysis of Spectral Hypercubes (FLAASH; Adler-Golden et al. 1999). Some approaches include more advanced features, such as spectral smoothing, topographic correction, and adjacency effect correction (Gao 2006).

2.3.1.3 Hybrid Approaches

The atmospheric correction methods mentioned above are isolated approaches, and each is tailored to specific conditions. A combination of those methods sometimes can yield

good results. For example, Clark et al. (1995) used a combination of ATREM and empirical line method to correct model errors in ATREM by calculating normalization factors of each pixel and then apply them to the ATREM corrected image. Some methods take advantage of ground measurements and MODTRAN to derive an equivalent model of empirical line method which has loose requirement on the uniform ground targets of different reflectance (Goetz et al. 1998). The best among these methods is the Empirical Flat Field Optimal Reflectance Transformation (EFFORT) that bootstraps a linear adjustment to apparent reflectance spectra to improve the accuracy (Goetz et al. 1997; Boardman 1998). The advantage of this method is that it improves the comparability of the corrected reflectance spectra with library-based spectra.

2.3.1.4 Data collection considerations with various atmospheric correction schemes

Field data may or may not be needed in atmospheric correction of hyperspectral images, depending on the analysis that will be utilized (Aspinall 2002). The IARR method requires no field data, which eliminates field data collection efforts at the expense of accuracy. The ATREM also does not need field data but is more accurate than IARR because it does require the sensor capability to capture narrow band width, especially in water vapor absorption bands. Flat field calibration only requires spectral data from one homogeneous site. Empirical line method requires a minimum of two high-contrast ground references sites although more references sites is preferable. MODTRAN requires extensive ground-based measurements and the information of atmospheric components, thermal structure and water content at different levels.

2.3.2 Geometric Corrections

Because the altitude of a flying plane is low enough to be affected by air currency, it is a challenge to keep the imaging platform steady. Image quality is not comparable to that of satellite platforms (Tong, et al. 2004). As a result airborne remote sensing imagery needs to be geo-rectified and registered to ground control points (GCP). This approach is expensive and time consuming due to the number of GCPs (Tong, et al. 2004). Most recent and advanced geometric corrections include Position and Orientation System / Direct Georeferencing (POS/DG; Reid, et al. 1998) supported by Global Positioning Systems (GPS) and Inertial Navigation Systems (INS) aboard the airplane. The combined system could provide information such as absolute position (x, y, z) and platform attitude parameters, which make it possible for real time geometric correction of airborne images using ray tracing to establish the relationship between the pixel and its ground counterpart.

Geometric correction is not necessary in this research for several reasons: (1) the weather on the image acquisition date was very pleasant which will ensure a more stable flight and good imaging quality, (2) the elevation in the research area is relatively stable, only a few meters difference negligible as compared to the flying height of the platform, (3) The image used in this research was geo-corrected with a C-Migits III GPS/INS unit manufactured by Systron Donner (CHAMP 2006). The system records GPS and aircraft attitudinal positions (roll, pitch, yaw, speed and heading). The rectification process uses the GPS and INS inputs to generate a global lookup table which is applied to the uncertified image (Tong, et al. 2004). The hyperspectral image matched very well with geo-orthorectified digital airphotos (DOQ).

2.3.3 Mapping and classification

Hyper-spectral imagery presents numerous possibilities for interpretation and analysis (Aspinall 2002). A lot of sensors have been developed which can provide a near complete spectrum for each pixel using high spectral resolution. Calibrated hyper-spectral data is comparable to laboratory spectra to identify ground materials at pure or mixed pixels. There are a number of specialized approaches tailored to hyper-spectral dataset that extract unique spectral features of different materials. Analysis of hyper-spectral imagery usually requires an empirical match between image spectra and reference spectra (end-members) from either a spectral library or field measurements.

2.3.3.1 Band ratio

Band ratio can be used to capitalize the spectral difference between different objects (Vincent 1997) to support the classification. Band ratios such as Normalized Difference Vegetation Index (NDVI) and Soil-Adjusted Vegetation Index (SAVI) have been defined in the literature to highlight vegetation properties (Elvidge and Lyon 1985; Huete et al. 1985; Huete 1988). The use of ratios also removes shadow effects caused by different angles of surface illumination. In multispectral remote sensing vegetation indices often use broad-wavelength red and near-infrared bands, such as Band 3 and 4 in Thematic Mapper (TM) images. Due to enormous pool of bands available in hyperspectral remote sensing, band selection is necessary before band ratio could be utilized.

Many approaches have been developed to select optimal bands in hyperspectral remote sensing images. Ifarraguerri (2004) measured a specific distance to all bands and then displayed the distances in image histogram to visually pick up optimal best bands. Huang

(2005) applied a more complicated band selection using feature weighting. It was based on the matrix coefficient analysis to assign weights to original bands then to select the bands with the largest weights. Keshava (2004) developed Band add-on (BAO) approach to exploit a mathematical decomposition of SAM to incrementally select optimal bands. This approach increases the angular separability between two classes of spectra.

Among these approaches, principle components analysis (PCA; Jensen, 1996) is the most popular one. PCA has been effectively used in multispectral data to reduce the number of bands by compressing bands into fewer, independent bands orthogonal to each other. The first component contains the largest variance that decreases with the sequence of components. The principle components transformation helps removing image redundancy with a de-correlation process. The inherent noise could also be reduced by excluding of low variance components.

2.3.3.2 SAM

The Spectral Angle Mapper (SAM; Kruse et al. 1993) matches pixel spectra to reference spectra using a similarity measure of angle, formed by the vectors of spectra in an n-dimensional space where n equals to the bands of image (Figure 2-2). In the SAM approach a smaller angle indicates a closer match. It is an exhaustive measure that compares each pixel vector with all available end-members and then classifies the pixel as the material with the smallest angle. The advantage of this approach is that it is insensitive to effects of illumination and albedo since only the angle between the vectors are measured instead of the length of them.

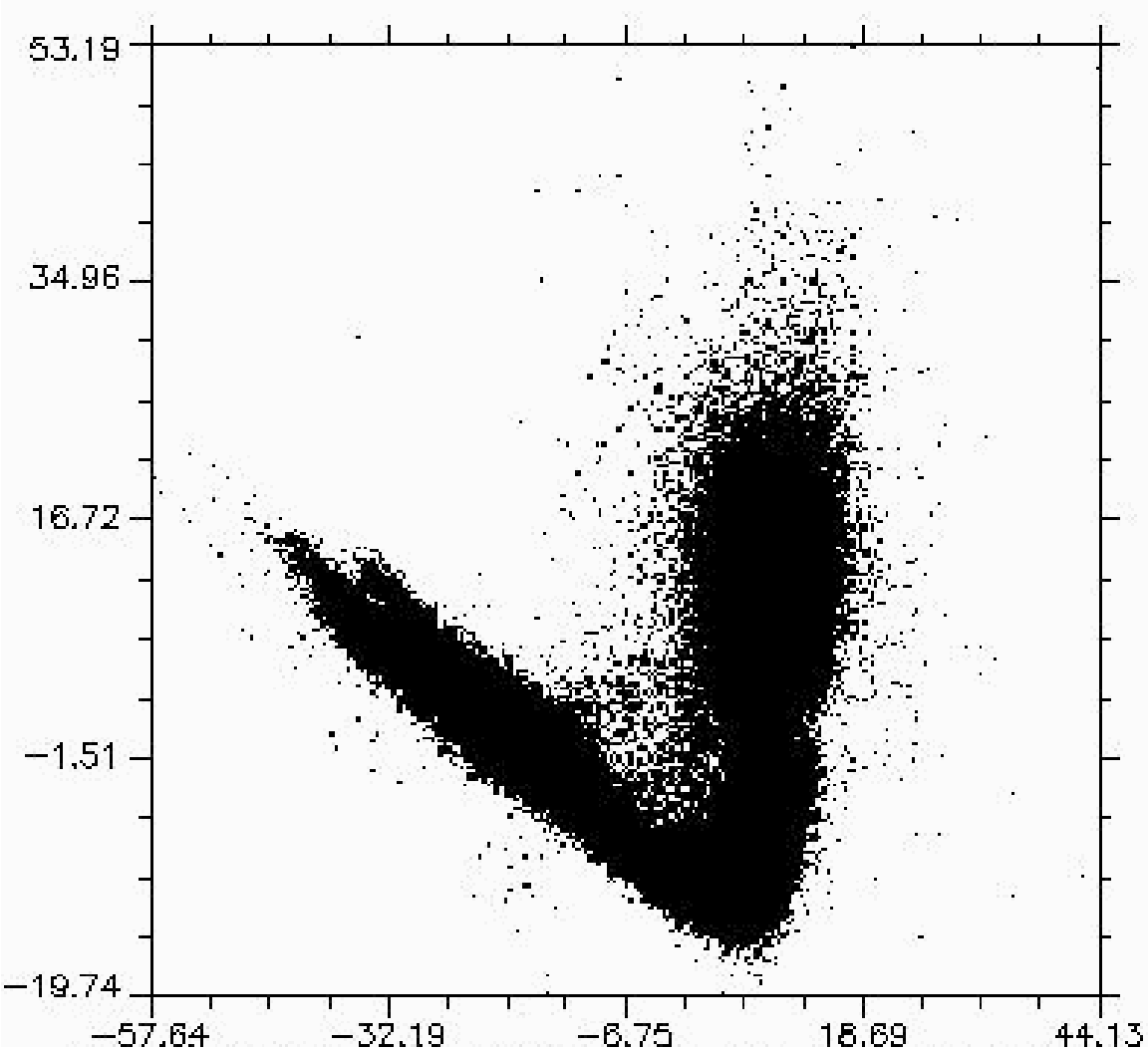

Figure 2-2: SAM algorithm illustration plot (ENVI 2002)

2.3.3.3 MNF and MTMF

Minimum Noise Fraction (MNF) was first introduced by Lee et al. (1990). This algorithm was developed to improve the principal components transformation's inability to reliably separate signal and noise components in multi-band images. The MNF was derived as an analogue of the principle components transformation which, instead of maximizing the variance of the data, maximizes the noise content of each component. Then it is reversed to obtain maximum signal-to-noise ratio (SNR) of each component. It is equals to transforming original data using noise covariance matrix as the identity matrix, followed

by a principle component transformation (Lee, J. B. et al. 1990). Mixture-Tuned Matched Filtering (MTMF) does not require the knowledge of all the endmembers. It maximizes the response of a known endmember and suppresses the response of the composite unknown classes (background) to match the known signatures (Chen and Reed 1987; Stocker et al. 1990; Yu et al. 1993; Harsanyi and Chang 1994). This approach is similar to un-mixing, but it does not require heavy computation as well as the knowledge of all the endmembers. This approach may introduce high commission error for pixels that are rare in the image (ENVI 2002).

MTMF is a hybrid method based on both signal processing and linear mixture theory (Boardman 1993). It combines the advantage of both the Matched Filter method explained above and physical constraints imposed by mixing theory to reduce commission error (Boardman 1993). MTMF results are presented as two sets of images, the Matched Filter image (MF) and the Infeasibility images with values from 0 (no match and feasible) to 1 (perfect match and infeasible). These results give a way to estimate relative degree of match to the reference spectrum and the Infeasibility image, where a high MF score and low infeasibility score represents a good match (ENVI 2002).

CHAPTER 3

METHODOLOGY

3.1 Study area and data collection

3.1.1 Description of the study area

Fieldwork was conducted within the Basket Area at the University of Missouri (UM-BWRA). It is located in southern Boone County about 30-minutes driving distance from campus (Figure 3-1). Although most of this 2,250-acre unit is covered by forests, there are some open areas where sericea patches in various sizes were observed. The study area is a piece of public grassland of the Cedar Creek Ranger District, Mark Twain National Forest (hereafter referred to as MTNF) inside the UM-BWRA (Figure 3-2). This field was selected because it represents less-managed public grasslands which have very high degree of sericea invasion. Since sericea spreads mostly in pastures and un-managed open lands, this study focuses on identifying sericea from surrounding grass. The study area is dominated by tall grass. Sericea patches in various sizes and height can be observed.

During field survey, ground sites of sericea and grass were selected. Depending on the dominance, the size of selected sericea patches varies but all sample sites were larger than 1×1 meter to be matched with 1-meter hyperspectral image. There are a total of 37 data collection sites in the study area, among which 12 are over grass and 25 over sericea.

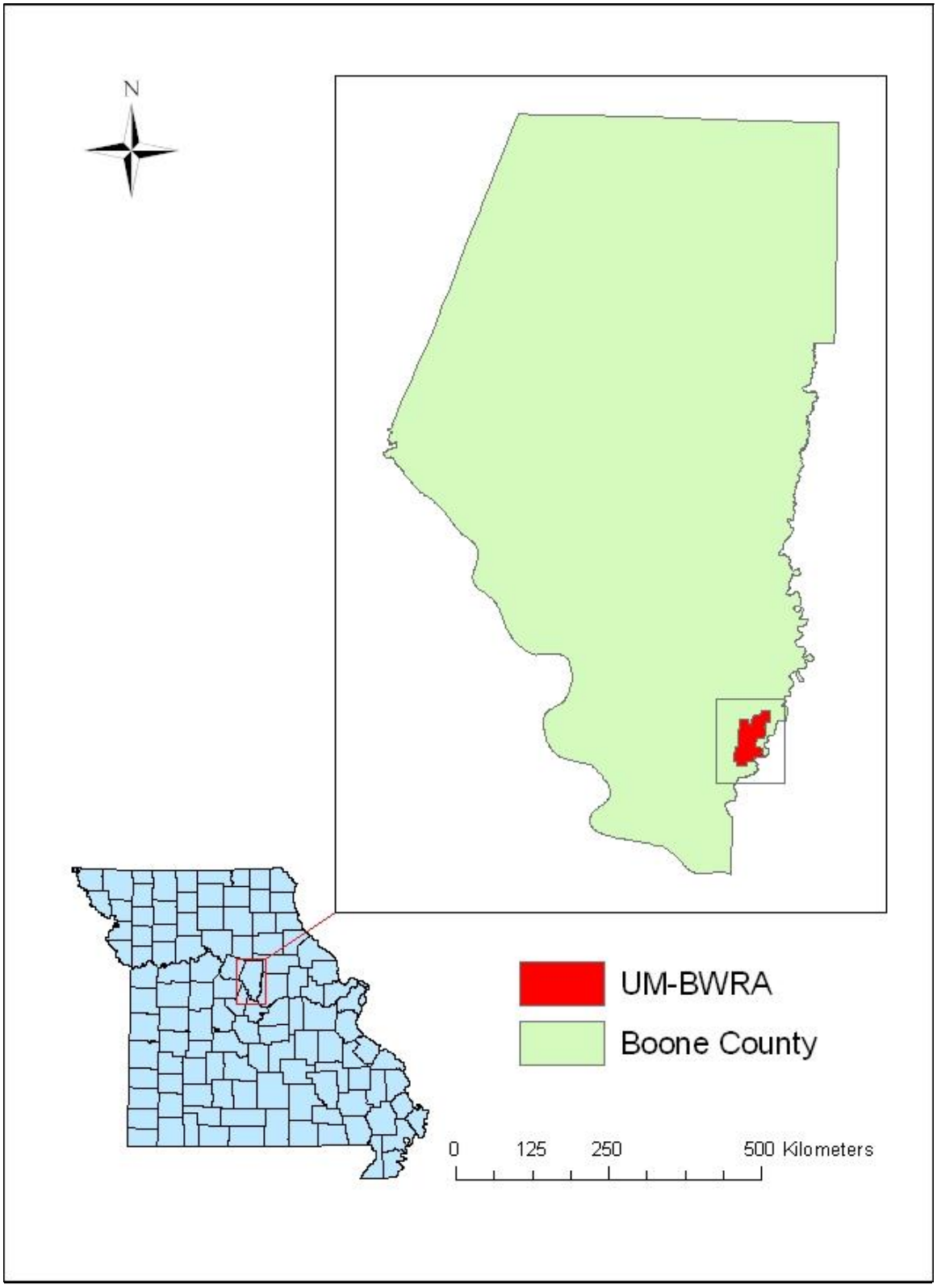

Figure 3-1: The Basket Wildlife Research Area (BWRA), University of Missouri

Figure 3-2: The study area is highlighted in the red box in this 2005 aerial photo of BWRA

Field survey and ground data collection was conducted by Dr. Wang (my advisor) and me on the following six dates: June 15, July 5, August 2, and August 24 2006. The August 2 data were used in this research because they are closest to the AISA imagery acquisition date of July 19. Data at other dates can be used for future research and they are also good sources for building spectral library of sericea at different stages of the growing season. Details of field data collection are discussed in the next section.

3.1.2 Field spectra acquisition (ASD)

A FieldSpecPro Full Range (FR) spectroradiometer from Analytical Spectral Devices, Inc. (ASD 2006) was used to measure reflectance (in the white reference mode) on the ground. Reflectance is the percentage of light reflected by a target as compared to the incident light on the same target. The rationale for using reflectance instead of radiance is because it minimizes the effect of different illumination conditions, thus allowing a better quantitative measurement of the ground object. To account for the variation of instantaneous illuminating conditions, white reference of a spectralon panel (which assumes a 100% reflectance) was collected several times during ASD data collection. The radiance measurements were converted to surface reflectance by dividing them with the white reference and recorded automatically in the field. The resulted reflectance ranges from 0.0 to 1.0 (0.0 stands for no reflectance and 1.0 stands for 100% reflectance). The ASD spectrometer unit incorporates 3 spectrometers to cover the whole range from 350 to 2,500 nm with a spectral resolution of 1 nm. Therefore it measures an approximately continuous spectral signature of the target. The spectra were collected at about 1.5 meter atop of the ground (Figure 3-3) during each field visit. The spatial distribution of the ground sites were displayed in Figure 3-4.

Figure 3-3: Data collection in field using the ASD spectroradiometer

3.1.3 Image acquisition (AISA)

One scene of the Airborne Imaging Spectrometer for Applications (AISA) hyperspectral image acquired on July 19, 2006 over the study area is shown in Figure 3-4. The image acquisition was through the collaborative effort of Dr. Harlan Palm (Plant Science Division, University of Missouri-Columbia) from his contract with the Center for Advanced Land Management Information Technologies (CALMIT 2006), in cooperation with the University of Nebraska-Lincoln (UNL) Department of Electrical Engineering and the University of Nebraska-Omaha (UNO) Aviation Institute. CALMIT's airborne remote sensing activities are centered on a suite of instruments associated with an AISA

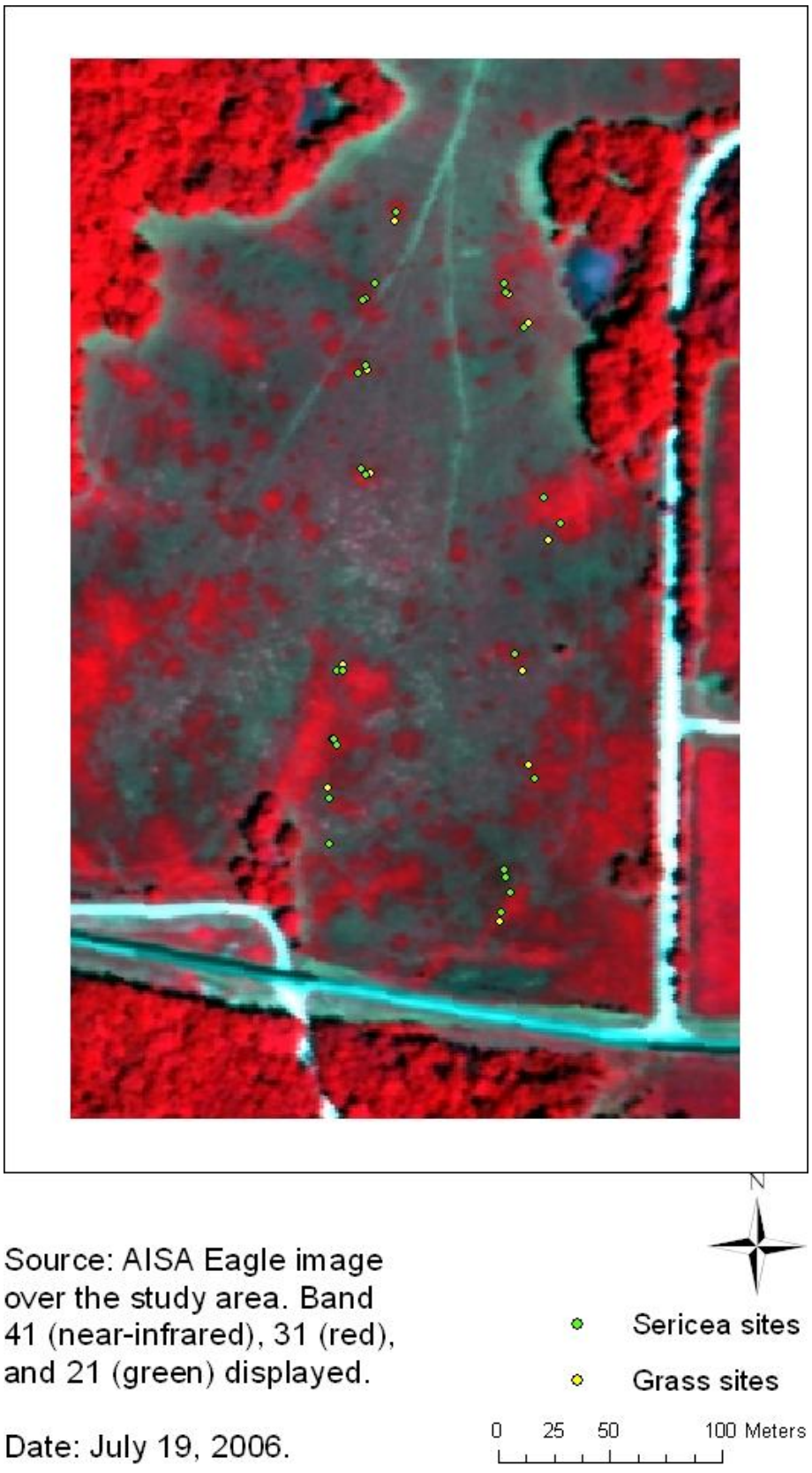

Figure 3-4: The AISA image and ground sites for ASD measurement

Eagle hyperspectral imaging system. This specific program is identified as CALMIT Hyper-spectral Aerial Monitoring Program (CHAMP 2006).

With a pixel size of approximately 1 × 1 m, the ASIA image covers a spectral region of 400-970 nm with an interval of approximately 9 nm which has considerable overlap with the ASD spectral characteristics. It contains 63 bands with a swath width of 520 m. The image delivered to us was radiometrically corrected and geometrically rectified. To reduce data size and computation time, only the subset area covering the MTNF field was processed in the following analysis. Figure 3-5 is a color cube of the subset image with the top layer shown in a color composition of band 31, 41 and 63 (as R, G, and B). Some features can be directly picked up via visual interpretation: (1) sericea is discerned by its brighter greenish color than grass, (2) trees are interpreted by their color and texture, (3) soil identified by its brownish orange color, and (4) different type of roads are discriminated by the color and the linear feature.

3.2 Data preprocessing

3.2.1 ASD spectra preprocessing

The ASD field spectra were analyzed in the Environment for Visualizing Images (ENVI) software (Version 3.6, Research Systems, Boulder, CO). A spectral library was built to store all field spectra. Later they were exported to ASCII format for further processing by ENVI, Interactive Data Language (IDL) software (a build-in programming language in ENVI), and Excel software (Microsoft, Seattle, WA).

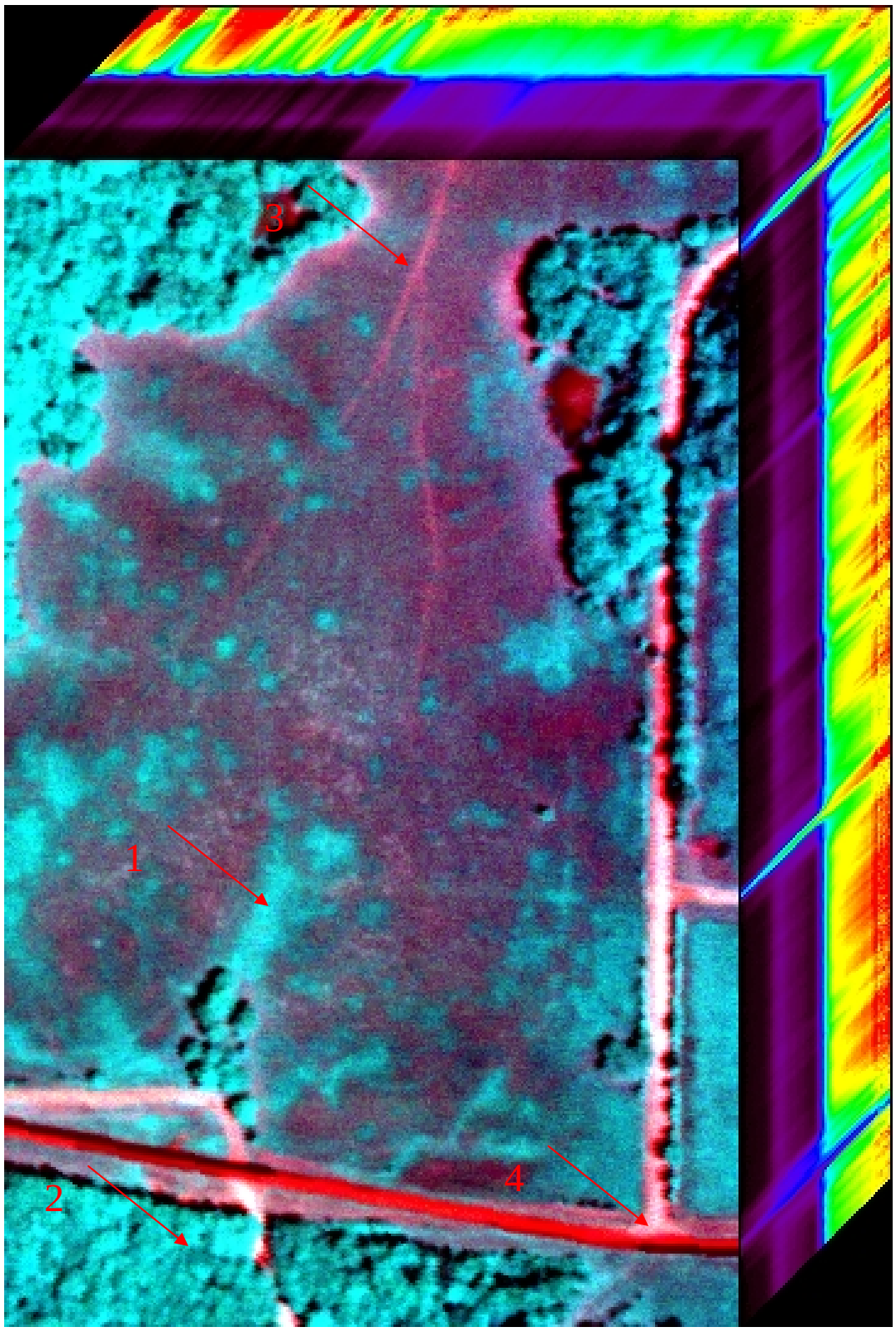

Figure 3-5: The AISA image cube with 63 bands, generated in ENVI software

3.2.1.1 Noise reduction

Noise in field spectra comes primarily from water vapor absorption in the air and the calibration error of the instrument. It obscures distinct spectral features such as reflecting peaks, and absorbing valleys of different target which makes spectral comparison between ASD measurement and the AISA image difficult. The ASD spectra need to be filtered to reduce noise while remaining the absorption and reflection features that are innate with the spectra of the target. Both Mean and Savitsky Golay (Sgolay) filter were used in the IDL program to smooth the spectra. The two filters were compared based on the criteria that it should smooth out high frequency noise while maintaining the smallest features associated with spectral features of grass and sericea.

The Mean filter is a simple approach which essentially does a local average on the spectra. The Sgolay filter is more complicated in that this method seeks to preserve the shape of reflectance peaks and absorption troughs. It performs a local polynomial regression to determine the smoothed value for each data point. An example of ASD field spectra is shown in Figure 3-6a. Noise in the forms of local peaks or troughs can be observed in the figure. A smoothed spectra based on Mean filter is displayed in Figure 3-6b and the one based on the Sgolay filter is shown in Figure 3-6c. It was found that the Sgolay method was superior to mean filter because it preserved local features of target that was lost in the mean filtered spectra.

Therefore, the Sgolay filter will be used in processing all the field acquired spectra to remove the noise.

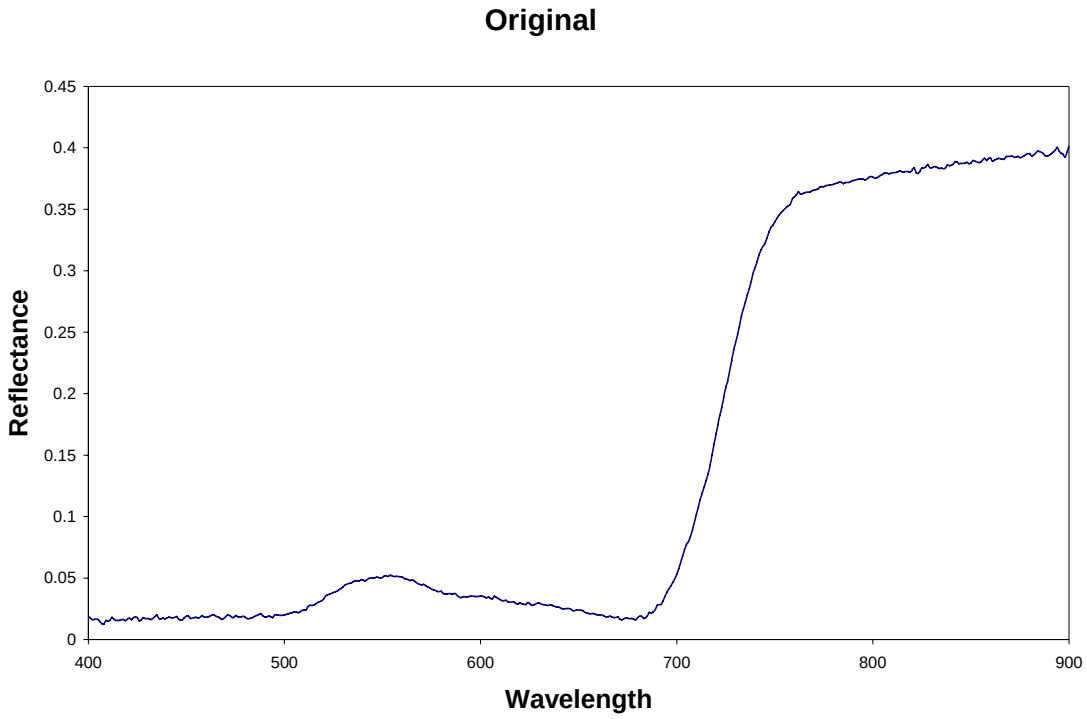

A: ASD spectrum

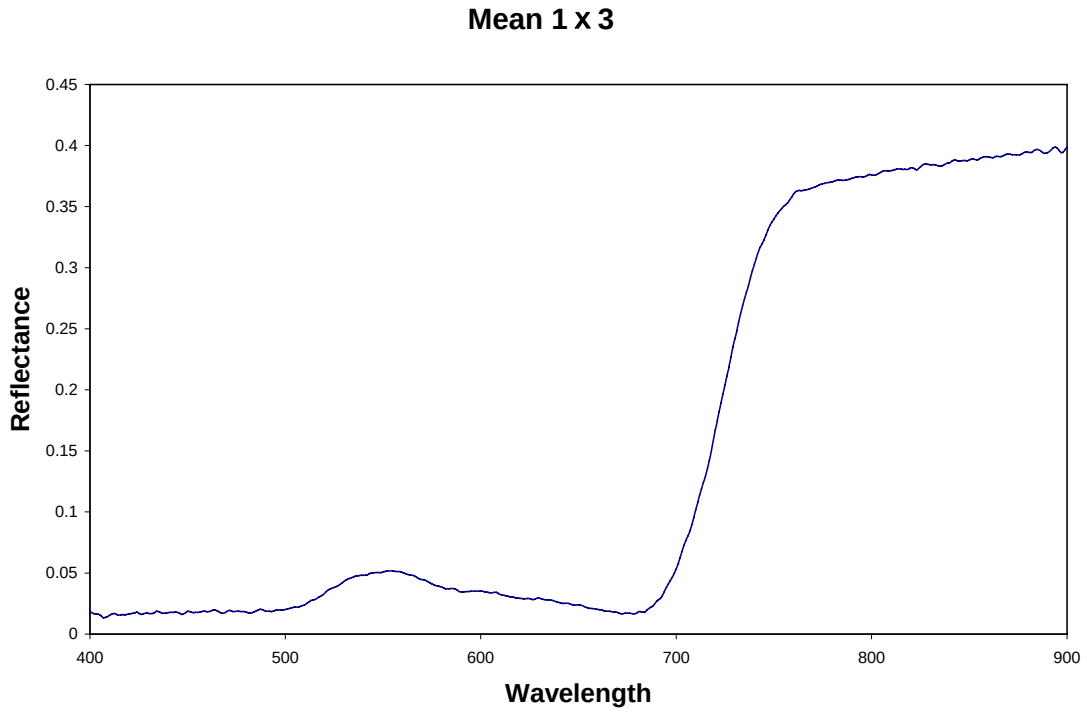

B: Mean filter spectrum

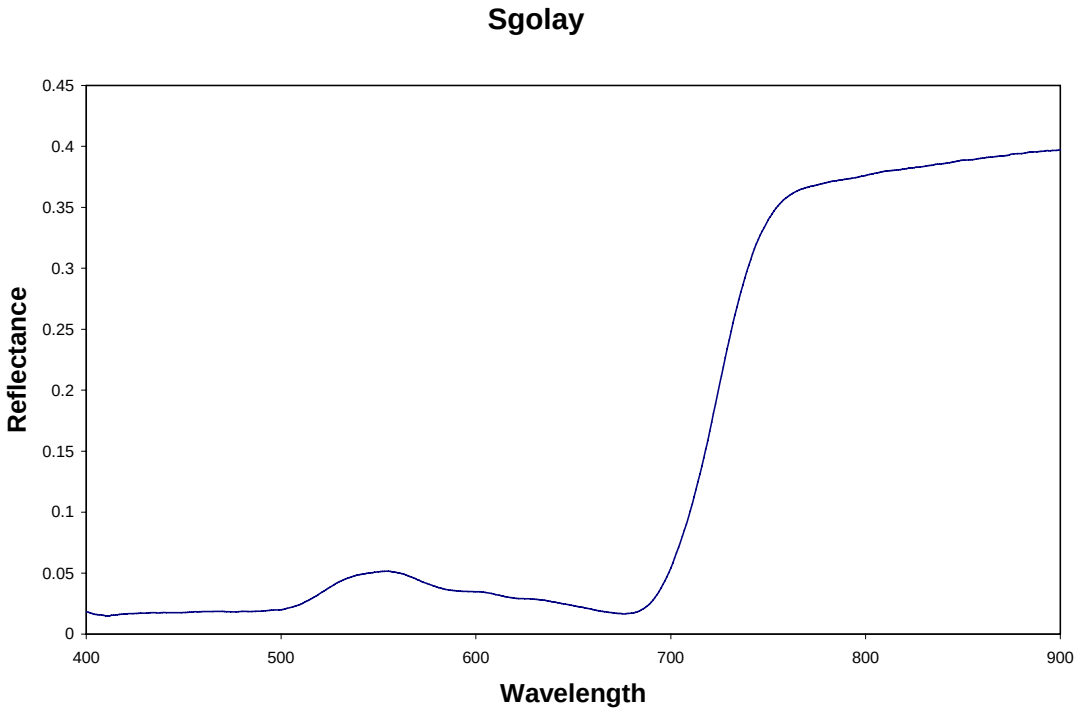

C: Sgolay denoised spectrum

Figure 3-6: Example of spectrum denoise procedures: (A) raw spectrum, (B) denoised spectrum with Mean filter, and (C) denoised spectrum with Sgolgy filter

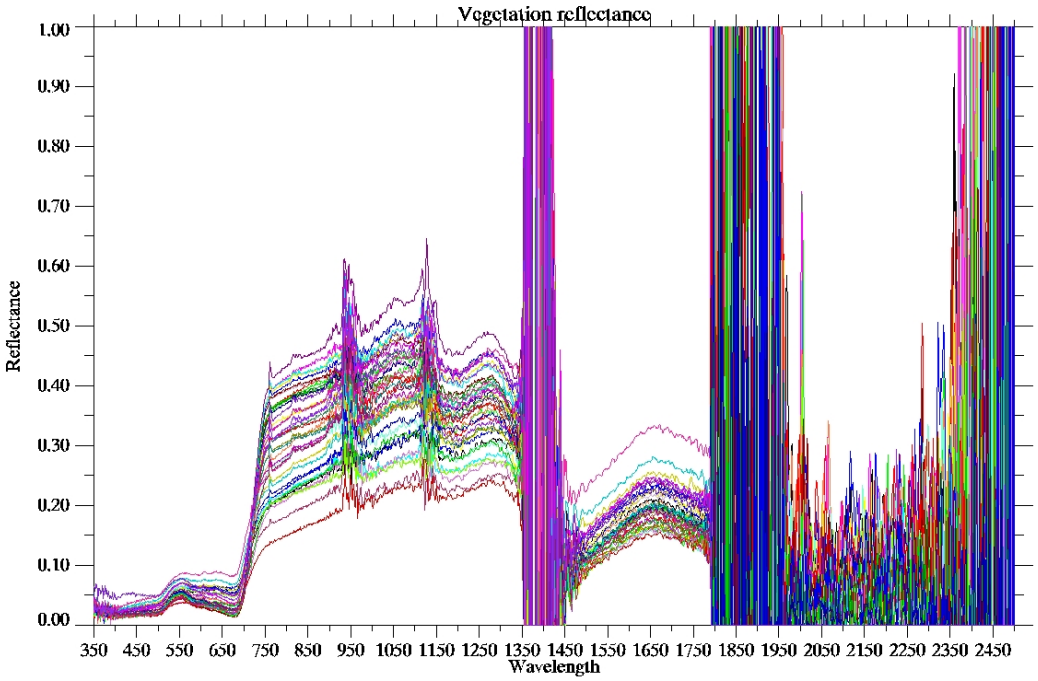

Figure 3-7: ASD spectral signatures (350 nm – 2,500 nm) at the 37 ground sites

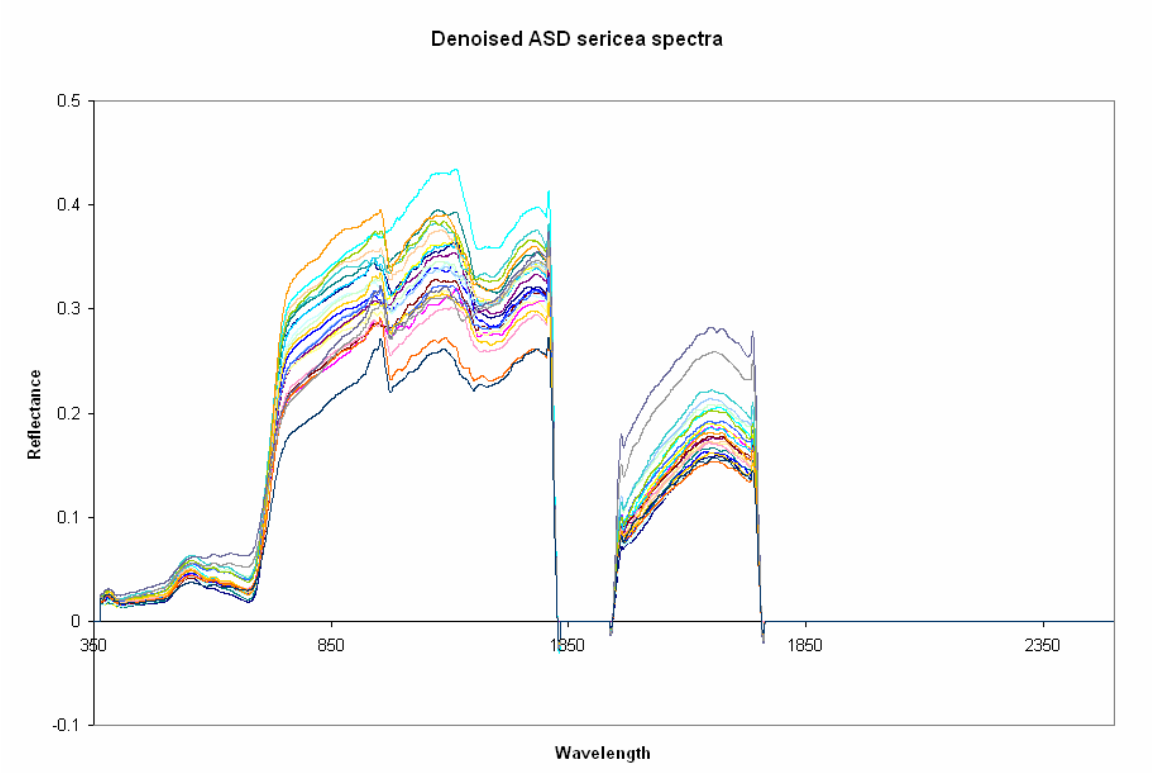

Figure 3-8: Denoised ASD spectra (sericea only)

The ASD spectra of all the ground sites are shown in Figure 3-7. The Sgolay denoised sericea spectra are shown in Figure 3-8, the wavelength regions dominated by noise are cut off manually before Sgolay denoising process. Compared with the original spectra, the denoised spectra are not only smoother but retain the spectral feature of the original ASD spectra.

3.2.1.2 ASD spectra resampling

The AISA image only has a spectral range up to 970 nm. Whileas the ASD spectra have a much wide range from 350 nm to 2500 nm. Thus the ASD spectra were cut and only the spectra in the range of 400-970nm were analyzed in the following processes (Figure 3-9).

The field acquired ASD spectra have a very high spectral resolution of 1 nm while the AISA image has a spectral resolution of 9 nm. The spectral resolutions in these two types of data have to be matched before they can be effectively compared with each other. There are two options for this process: (1) to down sample the ASD data to AISA data, or (2) to up sample the AISA data to ASD data. On one hand, up sampling of AISA data does not increase information and makes the AISA spectra bulky since certain range of wavelengths will have the same value. On the other hand, the AISA data have enough spectral resolution to satisfy the application need in this research. Therefore, the first approach (down sampling) was applied. The processing was performed in ENVI using the spectral resampling tool with AISA data as reference spectra and the spectra from previous steps as input.

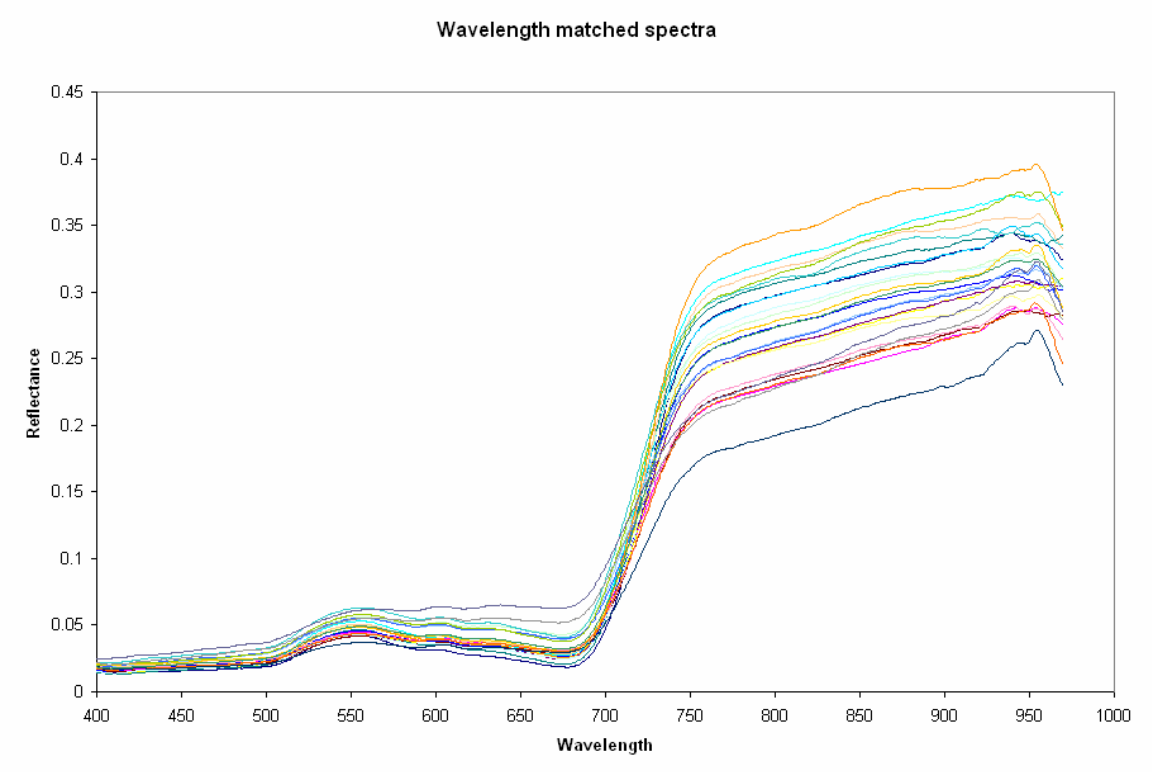

Figure 3-9: ASD spectral signatures in the range of 400 nm – 970 nm (sericea only)

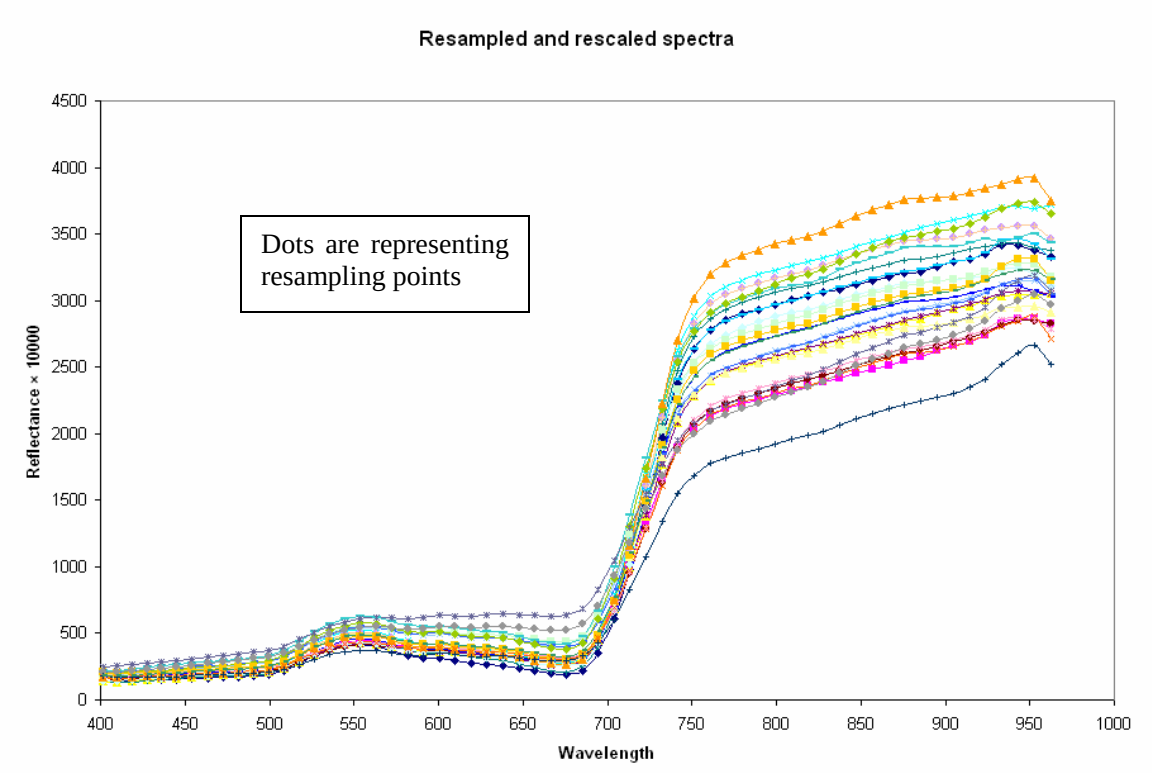

Figure 3-10: Resampled and rescaled ASD spectra (sericea only)

The ASD data were stored as decimal numbers ranging from 0 to 1, while the AISA data spectra were stored as integers ranging from 0 to 10000. Adjustments are needed to standardize their radiometric resolution. The ASD spectra were rescaled to meet the AISA radiometric configuration. The adjusted spectra are shown in Figure 3-10. The dots in the figure represent resampling points.

3.2.2 AISA Image Preprocessing

The AISA image has to be compared with ASD ground measurement for degree of similarity and conformity before it can be used in classification. The ASD spectra were collected on August 2 while the AISA image was collected on July 19. Although the weather was very nice on both days (very clear sky with few clouds) the different

atmospheric conditions could still play a vital role in the agreement between two dataset. To compare the similarity of these two datasets, spectra at each ground site were extracted from the image with the coordinates obtained during the field trip.

Pearson correlation was used to investigate the relationship between the airborne AISA spectra and hand-held ASD spectra at the same ground sites. The result shows very high correlation between ASD and AISA data with an R-square value of 0.9978 (Figure 3-11).

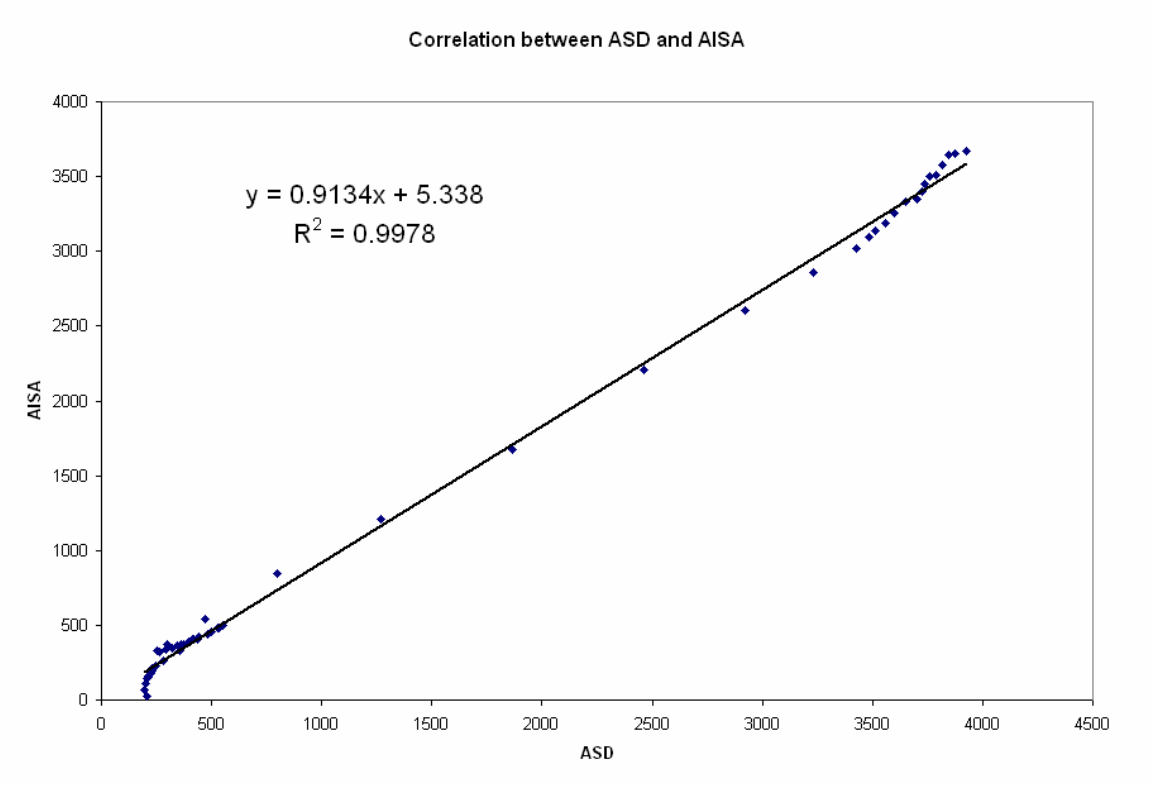

Figure 3-11: Correlation between ASD-measured and AISA-retrieved reflectance

The small yet existing inconsistency in the conformity between the two is probably due to reasons such as different date of data acquisition, cloud interference and system errors. Given the high correlation between them, ASD spectra will be tested in the classification. Image spectra will be used as alternative in case the ASD spectra are not effective in

classifying sericea pixels in the image. These two approaches each represent bottom-up and top-down approaches introduced in chapter two. Both of the approaches will be accessed and the better one will be used for final output. It is highly possible that top-down approach will be used in this research for reasons that vegetation spectra are so close and similar to each other and a little alteration can submerge the distinct signatures.

3.3 Image Classification

Several classification methods were investigated: (1) Band ratios, (2) SAM, and (3) MNF & MTMF. These approaches were compared based on the classification accuracy and cost effectiveness of their mapping performances.

3.3.1 Band Ratio

The normalized differential vegetation index (NDVI) using two optimal bands as red and NIR was calculated from the AISA image. The optimal bands were identified in the following band selection process.

3.3.1.1 Narrow-band (10nm) Indicator: band selection (reduction)

According to the Hughes phenomenon (Huges 1968), the classification accuracy first increases and then decreases when the feature space dimensionality increases but training data remain fixed. As a result, band reduction (selection) is crucial in information extraction of hyperspectral data (Mathur, et al. 2006).

The ultimate purpose of this research is to identify sericea from the surrounding,

predominant grass, in the study area. Here a Difference ratio ranking (DRR) approach was used to select the optimal bands which then served as input data to the classification. The rationale for this method is to compare the spectra between grass and sericea and then normalize the difference with either grass spectra or sericea spectra based on which class has higher reflectance in certain bands. Table 3-1 is a portion of the DRR band selection procedure. The red columns in the figure are the ratio difference between sericea and grass while the highlighted values in these columns represent the best bands for each ground sampling sites. The yellow rows stand for the two bands that have the most optimal bands for each ground sampling sites.

After the DRR process, the best two bands selected for band ratio classification are 676 nm (red) and 771 nm (NIR) (Figure 3-12).

Table 3-1: DRR band selection procedures

Wavelengt	G1	S1	DIF1	G2	S2-1	S2-2	DIF2-1	DIF2-2	G3	S3-1	S3-2	DIF3-1	DIF3-2
~	~	~	~	~	~	~	~	~	~	~	~	~	~
600.58	0.056784	0.034516	-0.39215	0.036409	0.044934	0.029436	0.189723	-0.19152	0.040131	0.030413	0.035097	-0.24216	-0.12544
609.98	0.055844	0.032448	-0.41895	0.036369	0.04245	0.028012	0.143251	-0.22978	0.039807	0.028749	0.033174	-0.27779	-0.16663
619.39	0.054677	0.02978	-0.45535	0.036156	0.039648	0.025541	0.088075	-0.29359	0.038668	0.02628	0.030215	-0.32037	-0.2186
628.79	0.054729	0.028577	-0.47785	0.036666	0.037874	0.024392	0.031895	-0.33475	0.03878	0.024763	0.028601	-0.36145	-0.26248
638.19	0.054471	0.026728	-0.50932	0.03675	0.035653	0.022983	-0.02985	-0.37461	0.038433	0.02346	0.026639	-0.38959	-0.30687
647.59	0.052805	0.023989	-0.54571	0.036065	0.03226	0.020746	-0.1055	-0.42476	0.03699	0.021049	0.023762	-0.43095	-0.35761
656.99	0.051054	0.021099	-0.58673	0.03505	0.028976	0.018593	-0.1733	-0.46953	0.035789	0.018478	0.020839	-0.4837	-0.41773
666.39	0.049051	0.018354	-0.62582	0.033566	0.025531	0.016421	-0.23938	-0.51078	0.034216	0.016201	0.017844	-0.52651	-0.47849
675.8	0.047935	0.017092	-0.64343	0.033128	0.023936	0.015074	-0.27747	-0.54496	0.033327	0.015379	0.016344	-0.53654	-0.50959
685.2	0.052533	0.021182	-0.59679	0.036658	0.028939	0.018294	-0.21057	-0.50095	0.037121	0.018563	0.020464	-0.49993	-0.44872
694.6	0.067938	0.038136	-0.43866	0.046833	0.049156	0.032781	0.047258	-0.30004	0.049294	0.033037	0.03777	-0.3298	-0.23378
704.02	0.091814	0.072385	-0.21161	0.062722	0.088943	0.062521	0.294807	-0.0032	0.069119	0.06525	0.072608	-0.05598	0.048053
713.45	0.118413	0.122818	0.035866	0.080227	0.144876	0.106872	0.446237	0.249317	0.093983	0.115751	0.123666	0.188059	0.240026
722.88	0.145458	0.188096	0.226682	0.097436	0.212879	0.163561	0.542294	0.404283	0.12364	0.184325	0.189107	0.329228	0.34619
732.31	0.168327	0.255642	0.341552	0.112324	0.279043	0.221039	0.597467	0.491836	0.152959	0.257742	0.256041	0.406542	0.4026
741.74	0.183844	0.308479	0.404031	0.123349	0.328185	0.265208	0.624148	0.534897	0.175764	0.316872	0.308755	0.445315	0.430733
751.2	0.194194	0.341335	0.431075	0.130905	0.358411	0.292736	0.634763	0.552822	0.191529	0.354715	0.342191	0.460048	0.440286
760.79	0.201094	0.358764	0.439481	0.136304	0.3749	0.307497	0.636426	0.556731	0.202209	0.37548	0.360533	0.461465	0.439139
770.4	0.204746	0.366298	0.44104	0.140095	0.381177	0.313795	0.632467	0.553546	0.207387	0.38315	0.367104	0.458732	0.435073
780.01	0.207442	0.370225	0.439687	0.143059	0.384647	0.317443	0.628077	0.54934	0.211114	0.386954	0.370689	0.454421	0.430482
789.62	0.210413	0.373067	0.435991	0.146379	0.38829	0.320689	0.623016	0.543548	0.215411	0.390775	0.374321	0.44876	0.424529
799.23	0.213719	0.375958	0.431535	0.14976	0.391534	0.323553	0.617504	0.537139	0.220027	0.39381	0.377008	0.441286	0.416386
808.84	0.21712	0.379081	0.427246	0.15305	0.394622	0.326261	0.61216	0.530897	0.225019	0.396746	0.380089	0.432839	0.407983
~	~	~	~	~	~	~	~	~	~	~	~	~	~

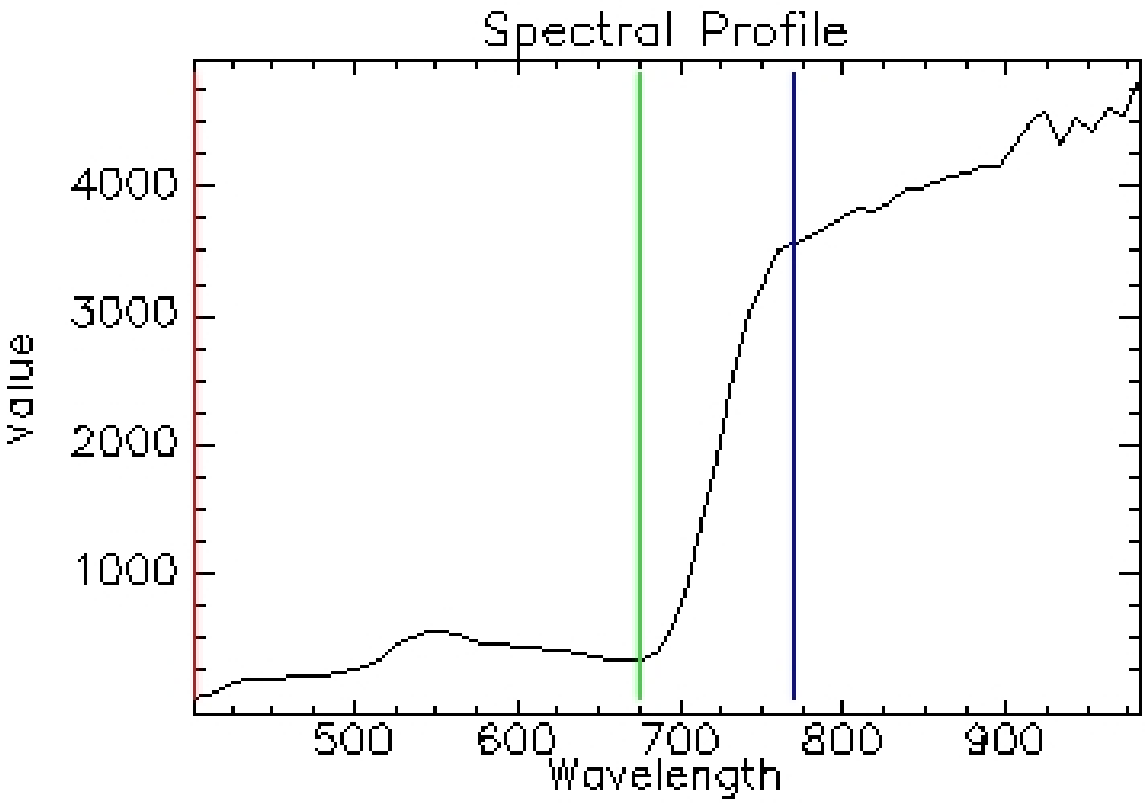

Figure 3-12: Band selection of the best two bands in red and near infrared region

3.3.1.2 NDVI image classification

The classification was done based on the manipulation of the histogram of the NDVI image. Level slicing was used to highlight sericea from grass, trees and other classes. Roads and bare soils were easily separated because they have very low NDVI value. The classification between sericea and grass was done in three controlled ways: (1) low commission error, (2) low omission error, and (3) medium commission and omission errors as in a balanced approach. The thresholds for those approaches are determined with sericea, grass and tree spectra. Due to the fact that averaged tree spectra will have a higher NDVI value than that of sericea which will have higher value than that of grass, four thresholds were selected (Table 3-2): highest possible grass NDVI (HG), lowest possible sericea NDVI (LS), highest possible sericea NDVI (HS), and lowest possible

tree NDVI (LT). The combination of those thresholds will ensure the described classification purposes are met. The HG, LS and HS values were determined from field measurement spectra plotted in graphs. The LT spectrum was obtained from image spectra because there were no ground spectra measurements available for trees. Due to operational consideration, the NDVI image was calculated in ENVI and then export to .lan format to be further processed in ERDAS (2005).

Table 3-2: Thresholds for different classification approaches

Thresholds	Low commission	Low omission	Balanced
Lower threshold	HG	LS	(HG+LS)/2
Higher threshold	LT	HS	(LT+HS)/2

3.3.2 SAM

The Spectral Angle Mapper (SAM) approach compares each pixel in the image with the endmember (spectrum represents a specific class) to decide which class it belongs to on the similarity (angle) between them. In order to have good SAM classification maps, several things need to be considered, they are: (1) classification approach (top-down or bottom-up), and (2) endmember selection. Both of them will be discussed in this section.

3.3.2.1 Classification approach

Unlike mineral identification, vegetation mapping faces more difficulties in separating different type of vegetation because they all have similar spectral response (Lamb and Brown 2001). In SAM approach the endmember selection is crucial to obtain accurate classification results. The field measured ASD spectra were tested and they turned out not

usable with SAM. Although they have high correlation with AISA spectra, the reflection peaks and troughs of the same target have different features at different acquisition dates which are deteriorated by the inaccuracies in atmospheric corrections. So a top-down approach is used in this approach. GPS coordinates of sericea from field work were used to obtain sericea spectra on the AISA image. These spectra were then used in the endmember selection process.

3.3.2.2 Endmember(s) selection

In the endmember selection process, it is suggested by Dennison (2003) that multiple endmembers can be selected to specify several sub-classes of target vegetation each representing different combination of patch density, patch size, and percentage cover that lead to the fluctuation of reflectance values in the spectra. The resulted sub-classes were then combined to obtain the final vegetation class map. The rationale of this approach is shown in Figure 3-13; the two green envelope spectra represent tree and grass while the red spectra represent different sericea spectral response. Multiple endmembers of sericea may be needed in the SAM algorithm in which the assigned threshold angle has to be very small to avoid between-class confusion close to the envelopes where different spectra meet.

Unfortunately this approach is not effective in this research. The specification of multiple endmembers will introduce gaps inside each sericea patch because data variation cannot be fully accounted for with such a small threshold angle. The logical way in solving this problem is to select the least number of endmember spectra as possible, say, to use one endmember; or to take a more complicated approach of specifying different threshold

value for different sericea endmember depending on their distance to other class spectra. The second alternative is very tedious and hard to achieve good result since it will involve a huge amount of adjustment, trial and error. So the first solution will be followed in this research.

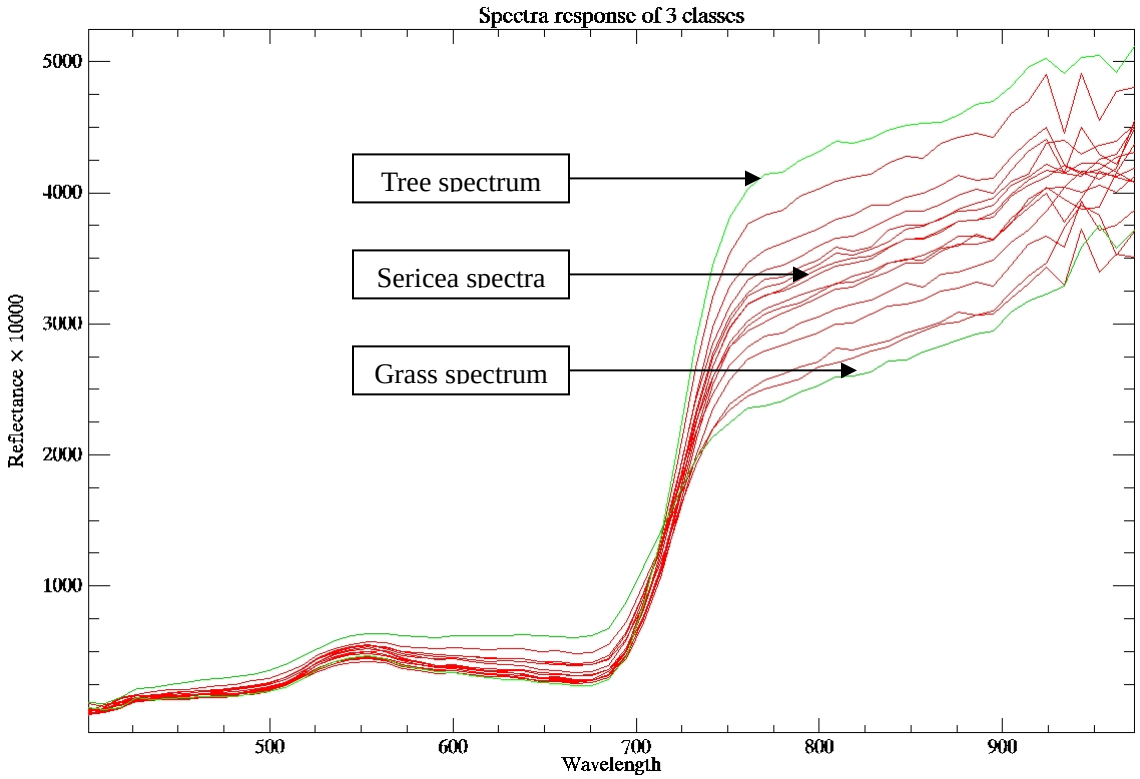

Figure 3-13: Illustration of endmember selection in SAM algorithm

We selected the average of all sericea spectra as the endmember. The average is a linear combination of all spectra of sericea, so it indirectly represents all possible sericea spectral signatures. The average spectrum also has least confusion with other classes because it has the farthest distance to different class spectra as far as all the sericea spectra are concerned. Using the average spectrum in SAM, the threshold could be set relatively larger until confusion happens between sericea and other classes, and only a limited number of trials could lead to good mapping and classification results.

3.3.3 MNF and MTMF joint approach

In this approach, a forward Minimum Noise Fraction (MNF) rotation will first be applied to the AISA image to get the MNF image and statistics. These statistics will then be used in the forward rotation of the endmember(s) to get the forward MNF endmember(s). The endmember selection in this approach is following the rationale of the SAM approach. So it will also be using averaged sericea spectra from the AISA image as the endmember, and only one endmember will be used.

In the MNF rotated image only the first 35 MNF bands were selected based on a 90% cumulative MNF variance (Glenn N. F. 2005). Then the subset MNF bands together with the forward MNF endmember(s) will be used as input in the MTMF mapping algorithm. The MTMF algorithm produces two values corresponding to each of the MNF pixel: (1) Matched Filter Value (MF); and (2) Infeasibility value both representing sericea. Pixels predicted to contain sericea were interactively selected from a scatter plot of MF value versus Infeasibility value. The criteria for this interactive process is to locate scatter plot pixels with relatively high MF value and low Infeasibility value depending on the application. Since the purpose of this application was to find all the possible sericea patches the pixels with both low MF and Infeasibility value will be considered. This approach will lead to slightly higher commission error which would ultimately lead to recommended over-spraying of herbicide on sericea. However, the omission error will be greatly reduced, and compared to the common practice of non-discriminatory spraying, a slight margin of over application than necessary can still be considered as environmental beneficial.

CHAPTER 4

RESULTS

4.1 Sericea mapping

This research tests three methods of image classification to determine the best means of identifying patches of sericea using remote sensing. Results from the first approach, band ratio, are very poor due to several factors: (1) the inability of band ratio to separate the confusion between tree, sericea and grass, and (2) the fact that ground spectra are only acquired from boundary of sericea in the protection of sericea patches. The second approach, SAM, produces much better results, effectively identifying sericea patches, but confusion with trees still exists. The best approach found is the MNF & MTMF joint approach. Not only are the sericea patches identified accurately but the confusion with trees is kept to a minimum with the help of a majority filter. The details of these mapping results are presented in the following sections.

4.1.1 Band ratio

4.1.1.1 Threshold identification

The grass NDVI values corresponding to field grass sites are plotted to identify the highest grass NDVI value (HG) in Figure 4-1. In the same way, the highest sericea NDVI (HS) and lowest sericea NDVI (LS) are identified in Figure 4-2. Due to the lack of ground data, the lowest tree NDVI (LT) is identified in the NDVI image (Figure 4-3).

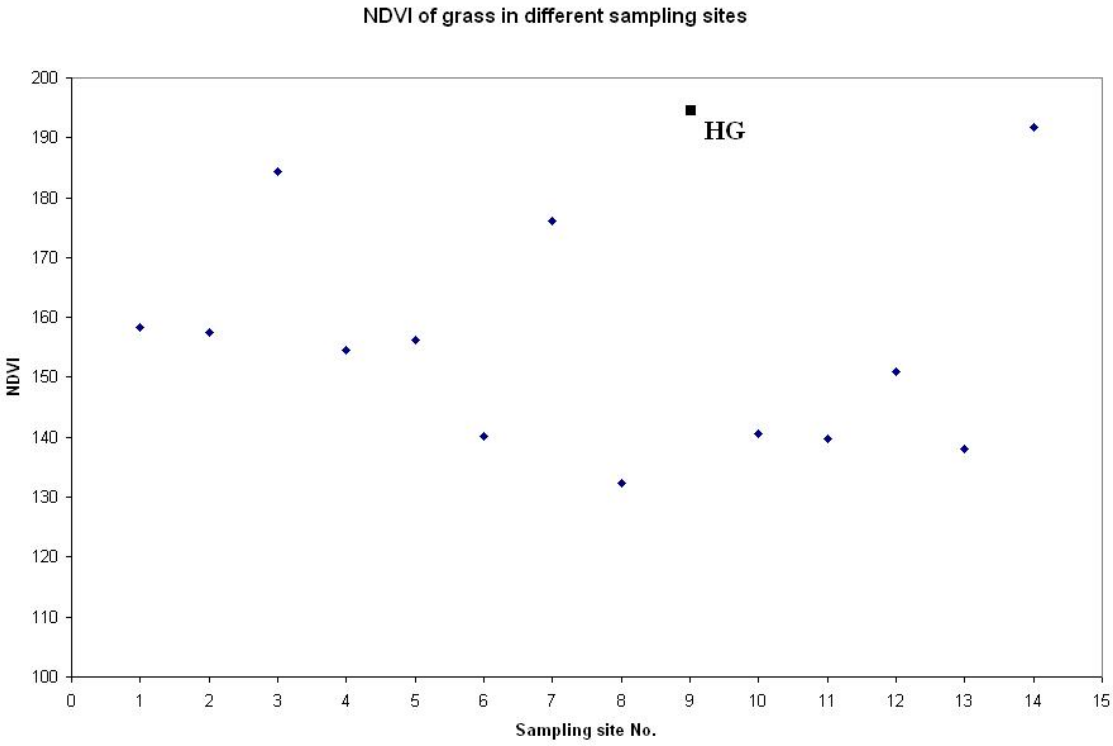

Figure 4-1: Highest possible grass NDVI value

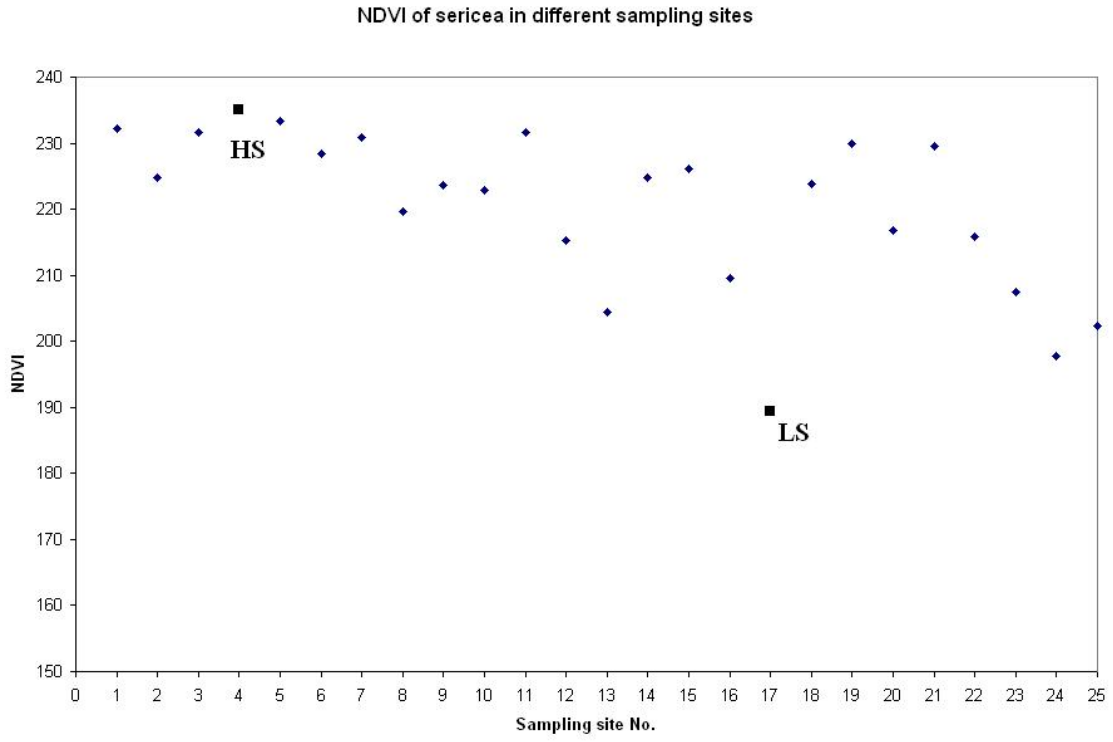

Figure 4-2: Highest and lowest possible sericea NDVI value

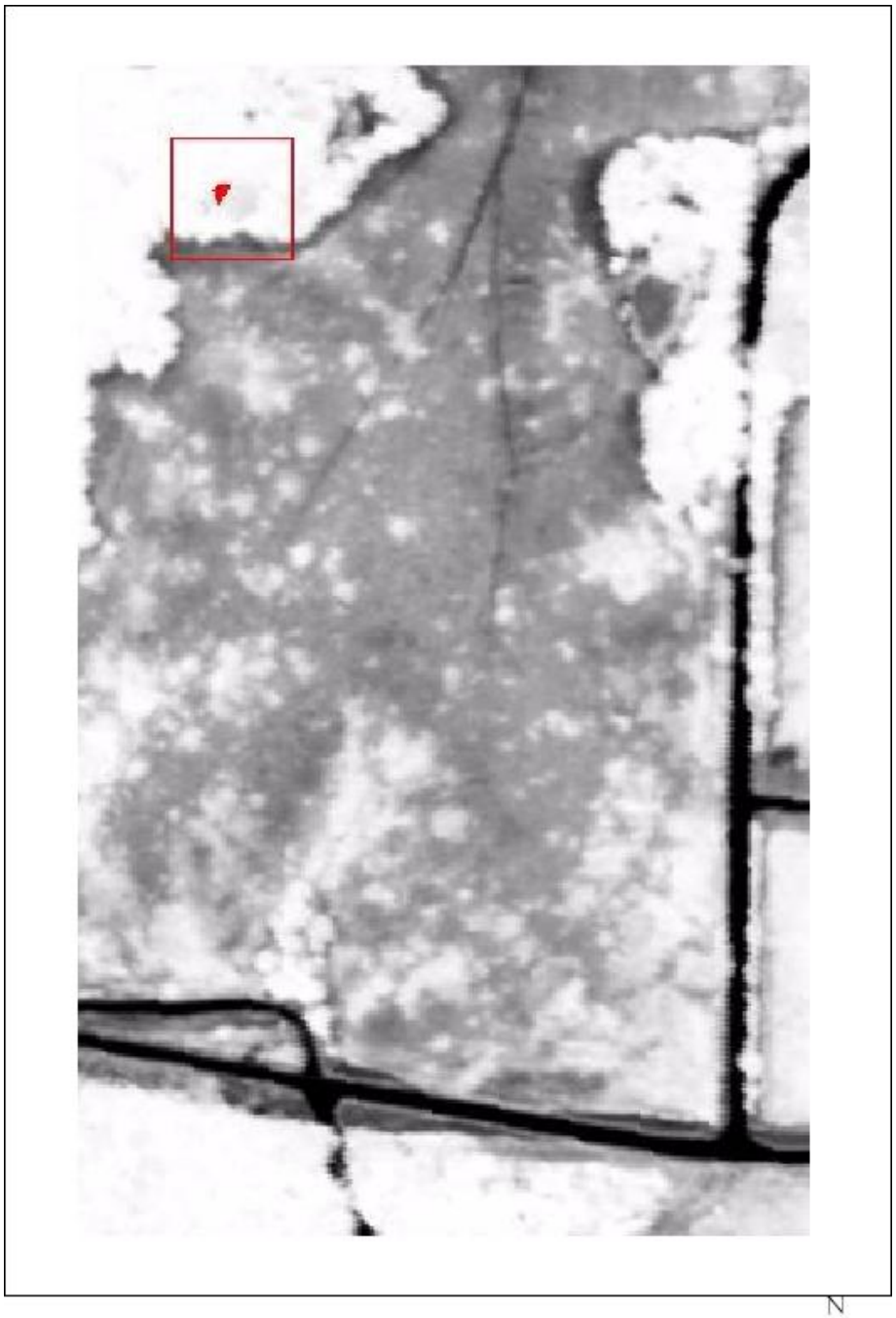

Figure 4-3: ROI for obtaining Lowest NDVI of tree

4.1.1.2 Low commission error approach

The two thresholds identified as High Grass (HG) and Low Tree (LT) are 195 and 221 as shown in breakpoint editor of ERDAS software dialogue (Figure 4-4).

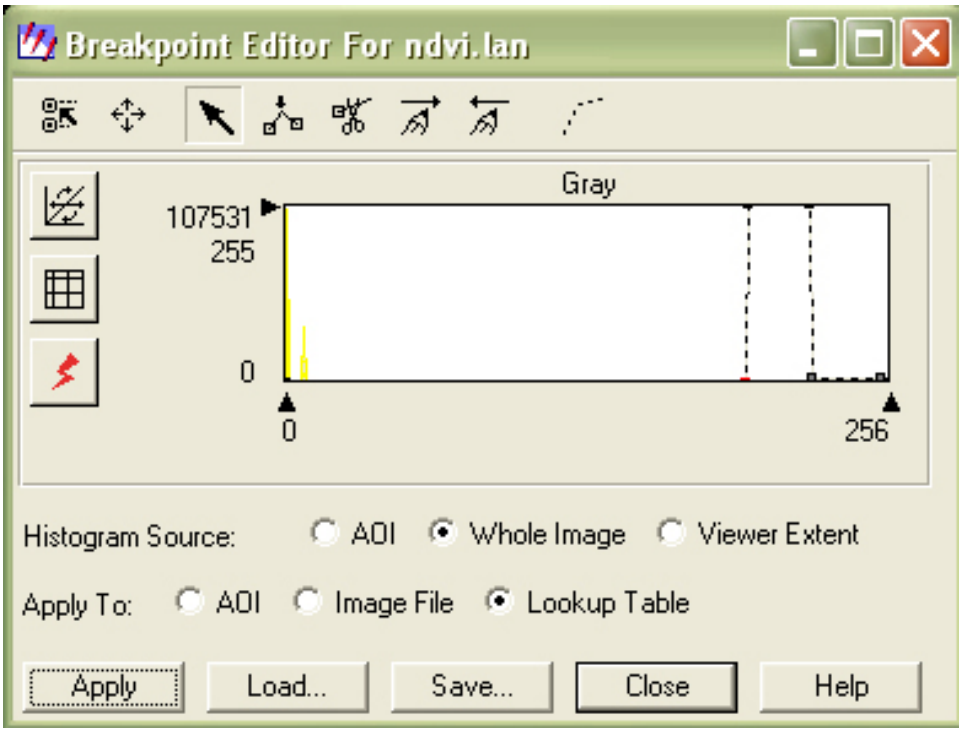

Figure 4-4: Low commission thresholds shown in the breakpoint editor

The low commission error approach as shown in Figure 4-7 managed to rule out the influence of other classes especially tree class since only a very small portion of trees is highlighted in the class map. But it failed to identify sericea patches; instead it outlines the boundary of sericea patches which may need further work and human interference to fill the patches to come up with a better output of sericea map.

4.1.1.3 Low omission error approach

The two thresholds identified as Low Sericea (LS) and High Sericea (HS) are 189 and 235 as shown in breakpoint editor of ERDAS software dialogue (Figure 4-5).

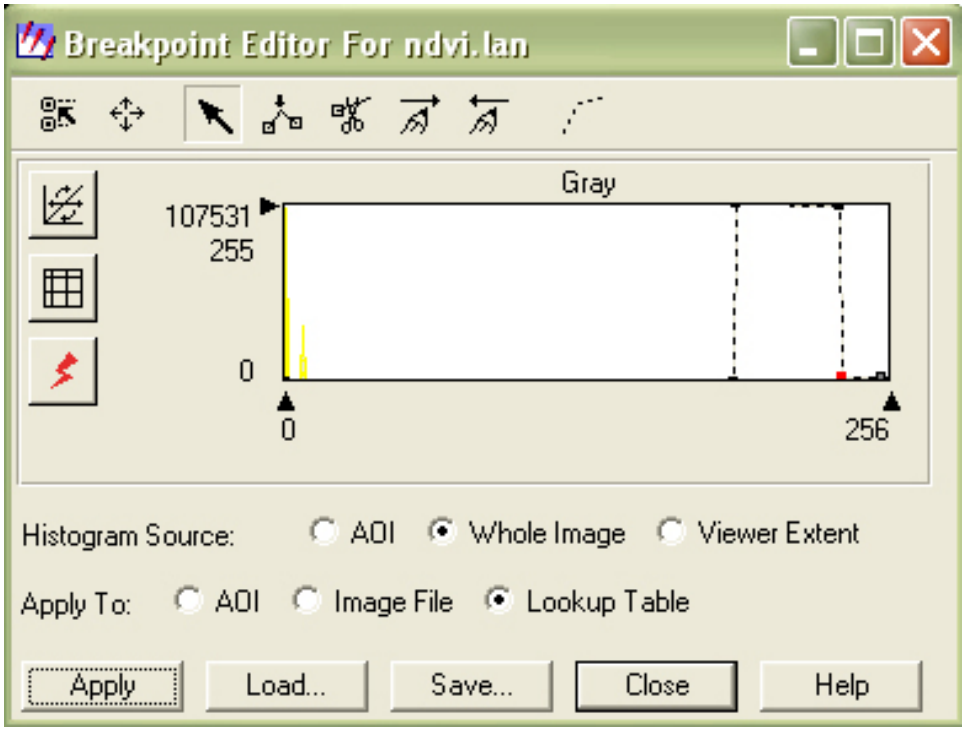

Figure 4-5: Low omission thresholds shown in the breakpoint editor

The low omission approach in Figure 4-8 included more tree classes and overestimated the boundary of sericea but still was not able to pick up the whole patches of sericea. The cause for this problem is bi-fold, (1) the field measured sericea spectra is not representative enough to cover the whole range of possible sericea spectra; and (2) the NDVI of sericea has so wide range of values that cause the confusion with other vegetation. The first cause is partly due to the fact that field spectra are only acquired at the boundary of sericea patches in the protection of the uprightness of sericea, since once stepped on the sericea will have different spectral response because of a different looking angle. This problem could be solved by either acquiring field data with a certain mechanical device that could stretch the ASD pistol to be above the middle of a sericea patch or by acquiring mid-patch spectra from ROI tool applied on the image. The second problem is more difficult to tackle, and probably the only way out of it is to either use the

balanced approach and tolerate the relatively low accuracy of classification or explore other band combinations that have fewer between class confusion.

4.1.1.4 Balanced approach

The two thresholds as the average of commission and omission approaches are 192 and 228 (Figure 4-6).

The balanced approach as shown in Figure 4-9 also has the problem as the low commission error approach does. Therefore, it seems narrow band indicator is not very effective in picking up whole sericea patches.

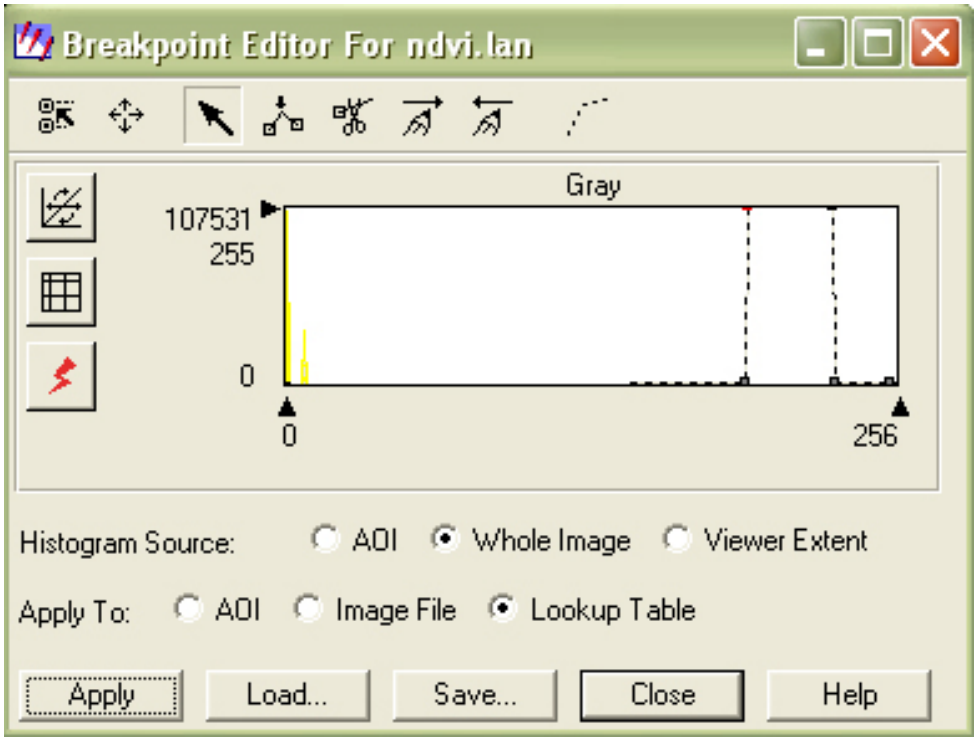

Figure 4-6: Balanced thresholds shown in breakpoint editor

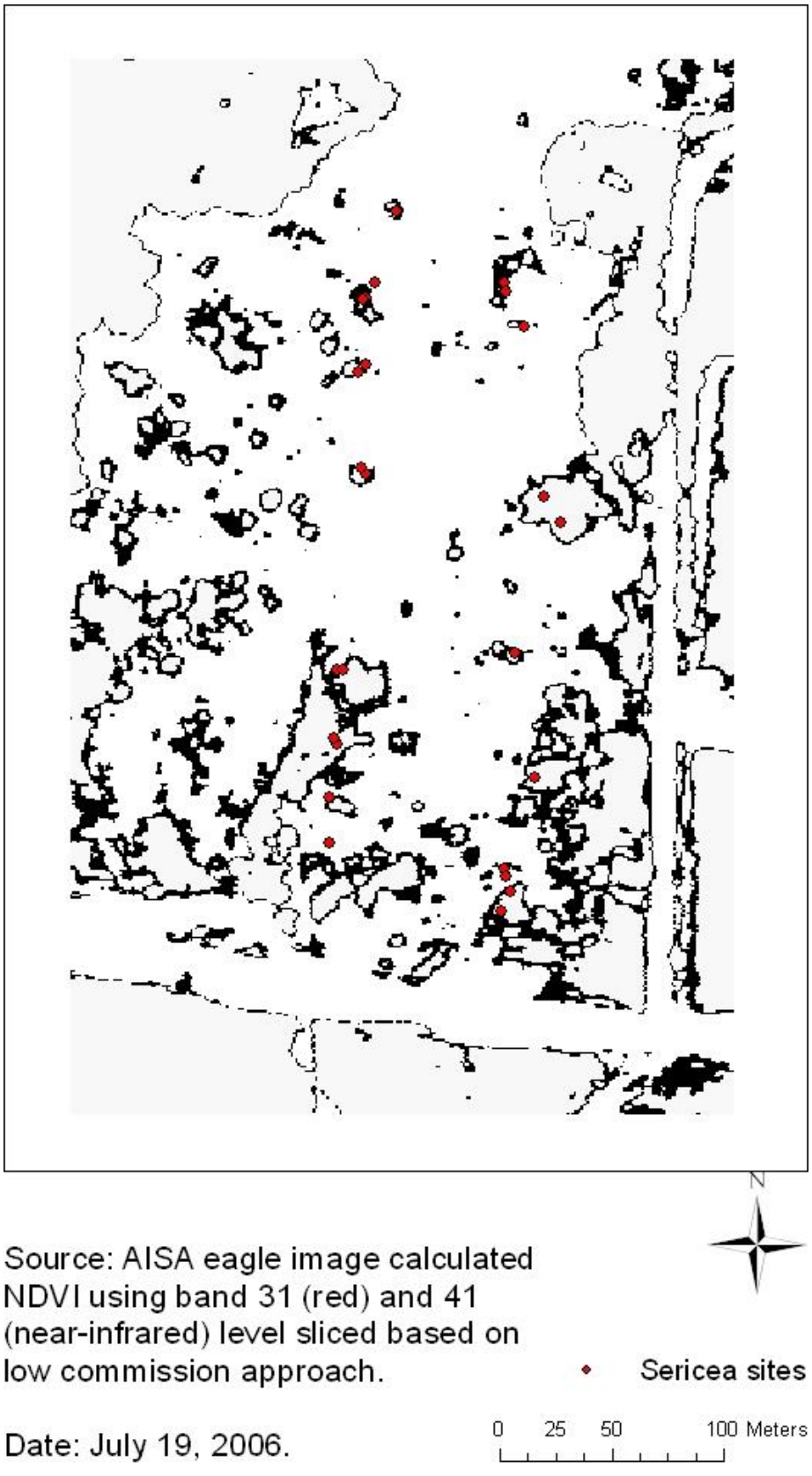

Figure 4-7: Sericea map with low commission approach

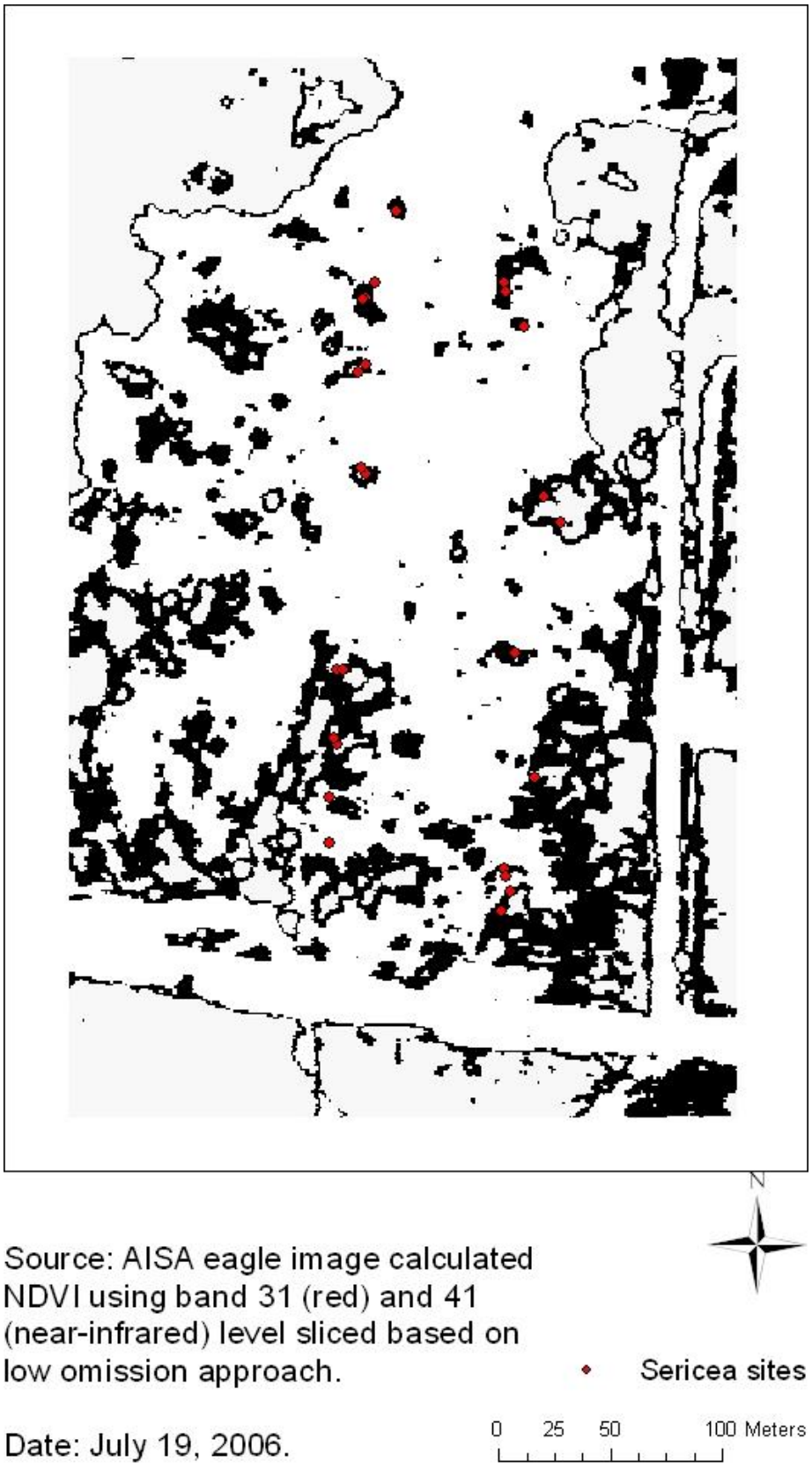

Figure 4-8: Sericea map with low omission approach

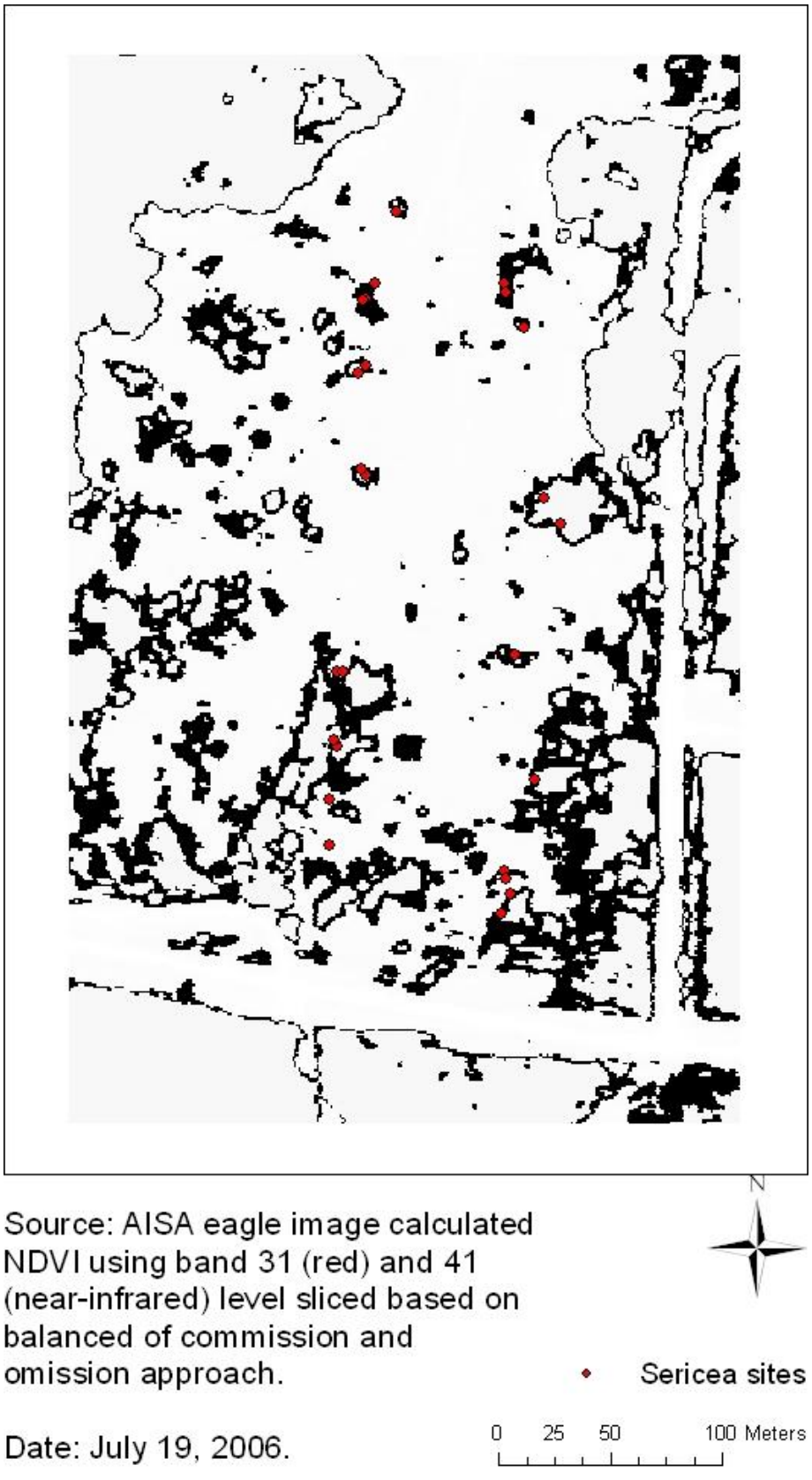

Figure 4-9: Sericea map with balanced commission and omission approach

4.1.2 SAM

The endmember spectrum used in the SAM classification is shown in Figure 4-10.

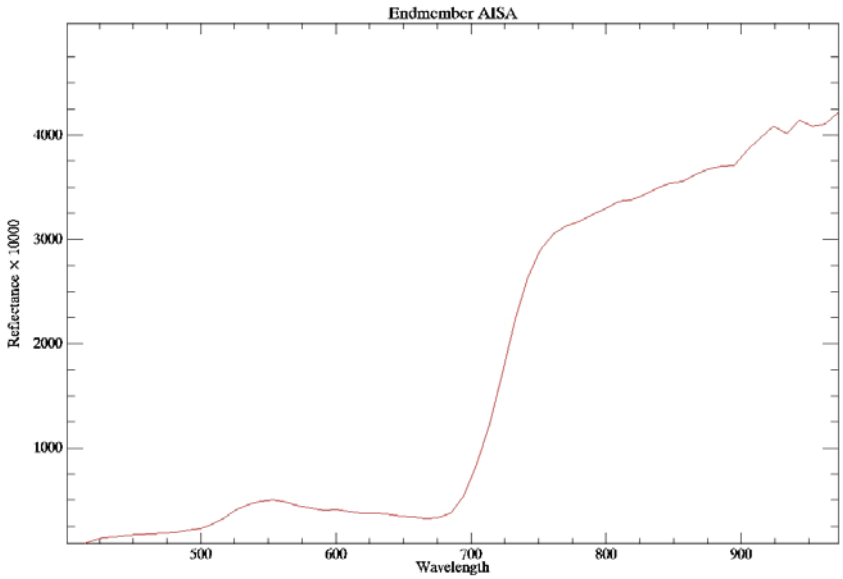

Figure 4-10: SAM endmember (averaged sericea spectrum)

Various threshold angles have been tried with the SAM approach and only one was applied in this research and described below. Two maps with different threshold values in SAM classification were shown in Figure 4-11 and 4-12. Figure 4-11 uses 0.03 as the threshold angle which is very effective in depicting sericea patch without much confusion with other vegetation such as trees, but it results in relatively high omission error. Although most of the sericea sites fall inside the classified sericea patches, there are a lot of sites fall outside of the patches (Figure 4-11). Figure 4-12 uses 0.04 as threshold angle which turned out very good sericea patch delineation, less sericea sites fall outside the classified patches, but it results in high commission error. Because a lot of obvious tree patches are classified as sericea. Since the threshold change from 0.03 to 0.04 does not increase sericea patches significantly and introduced a lot of confusion with trees. Only Figure 4-11 was used in accuracy assessment.

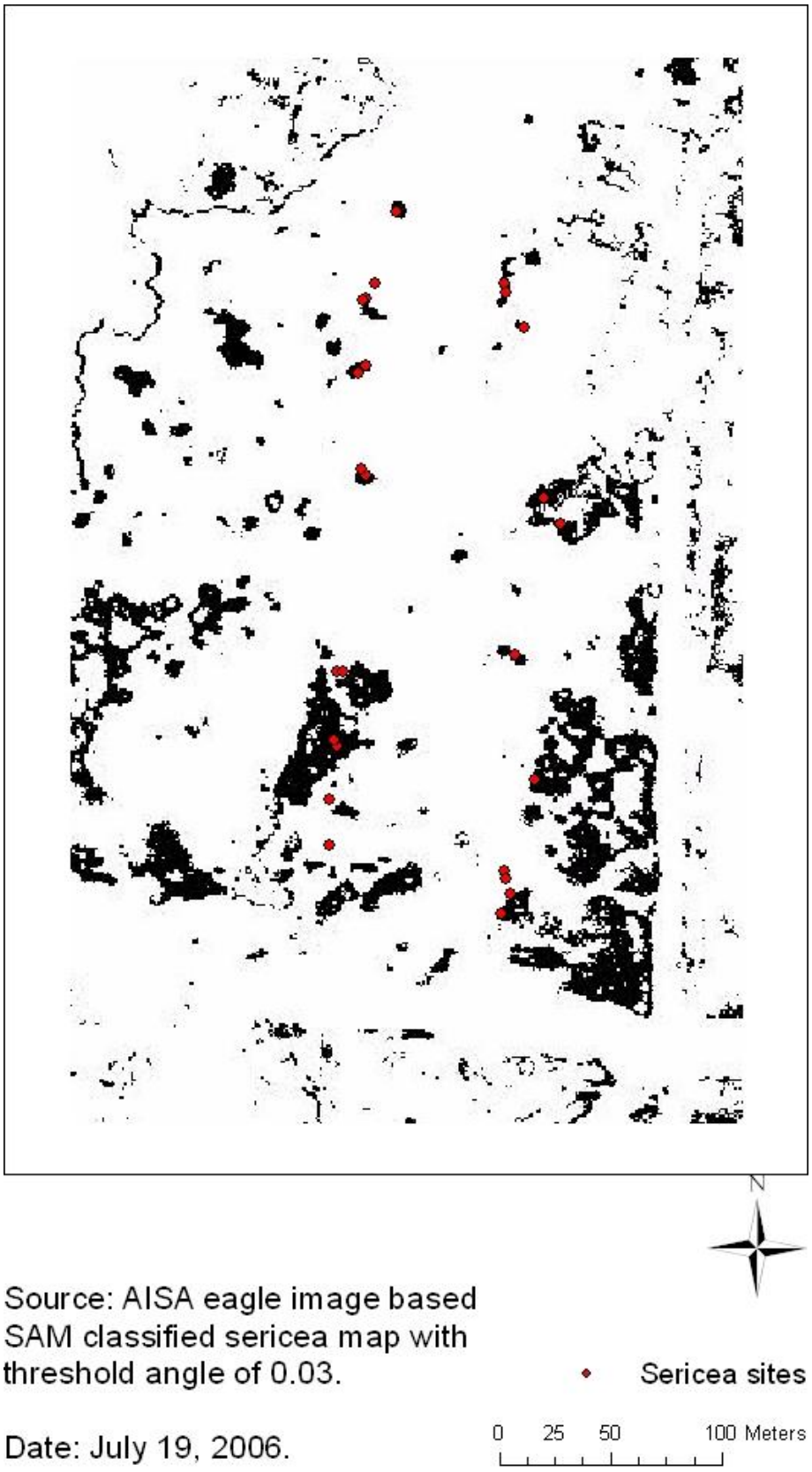

Figure 4-11: SAM sericea map at threshold angle of 0.03

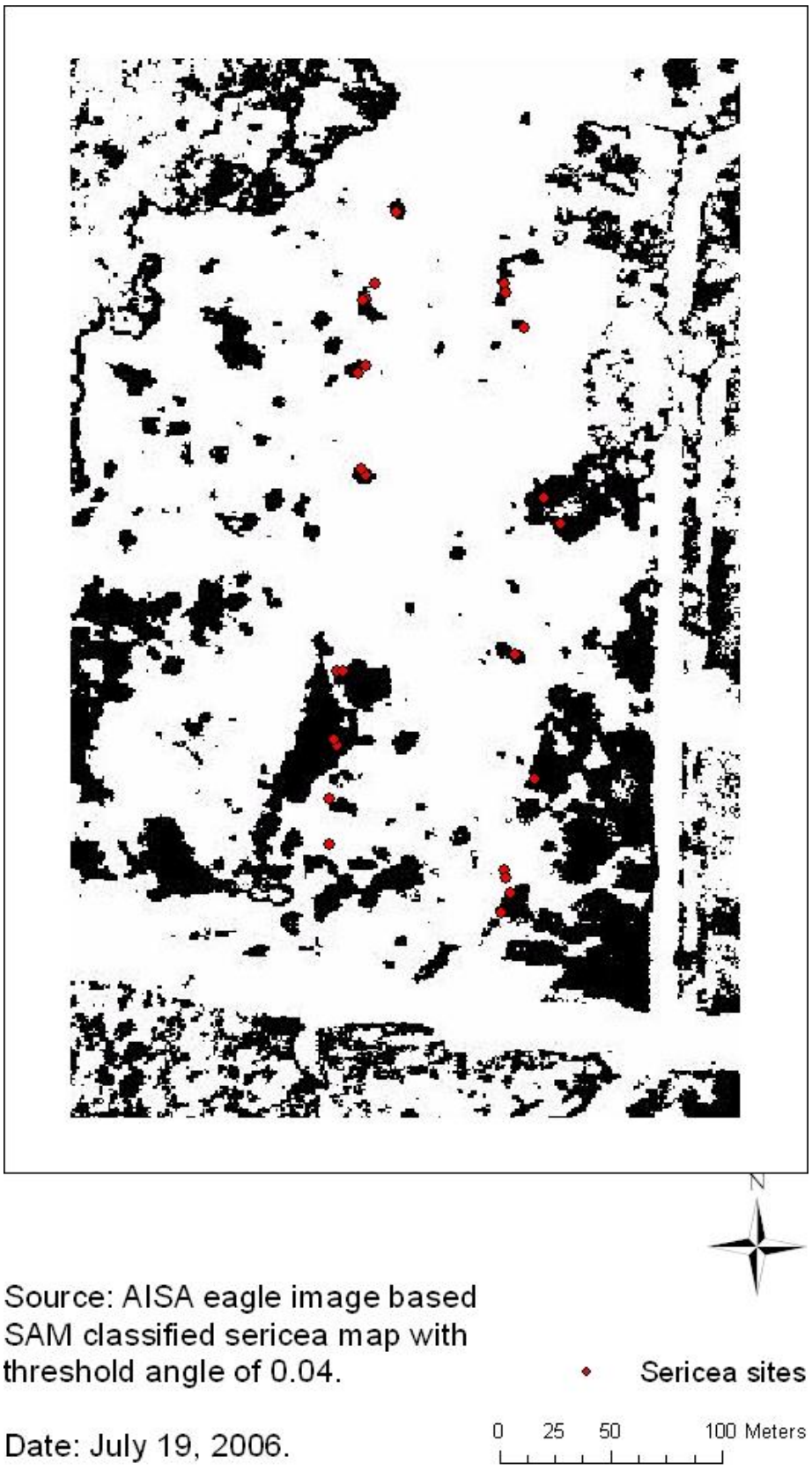

Figure 4-12: SAM sericea map at threshold angle of 0.04

4.1.3 MNF and MTMF

4.1.3.1 MNF Image and endmember

Figure 4-14 is showing the effectiveness of MNF transformation that different vegetations all showed up in different colors. Especially the sericea patches that are showing very light greenish color that are very different with other colors representing different vegetation classes.

The statistics by-product of MNF transformation of the image is used in forward rotation of the sericea endmember spectrum. The MNF rotated endmember is shown in Figure 4-13. The sudden reduction in oscillation on the value is showing that most of the data variation was contained in first a few bands. But more bands will be used in MTMF mapping to satisfy the criteria of a 90% cumulative MNF variance (Glenn N. F. 2005).

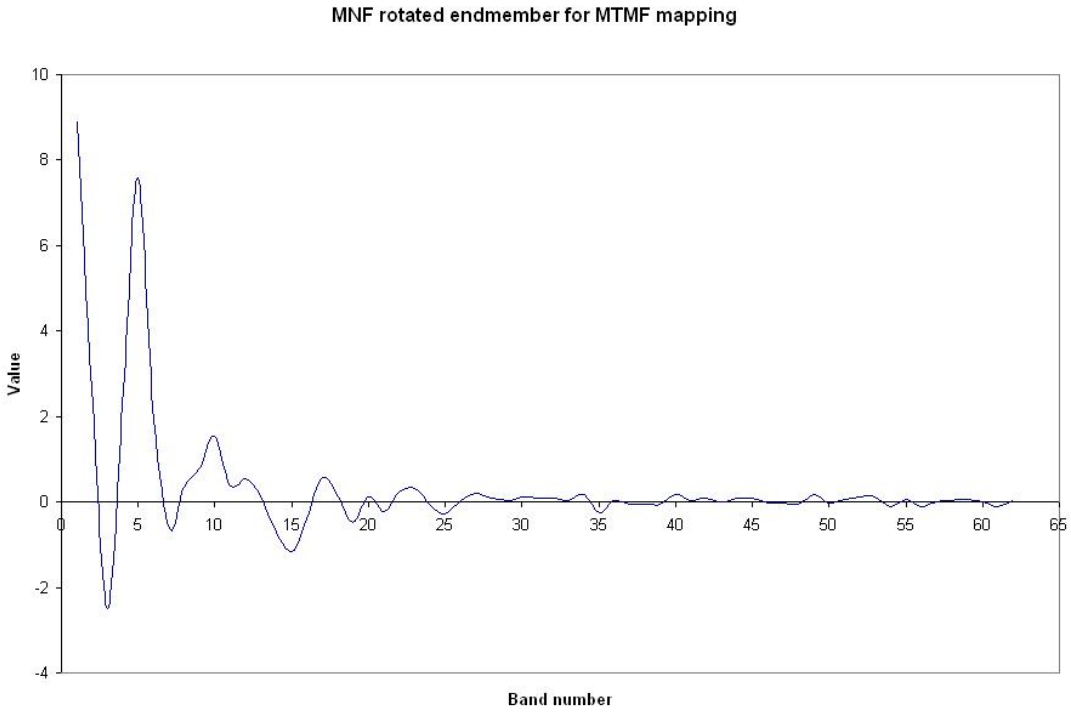

Figure 4-13: MNF rotated sericea endmember

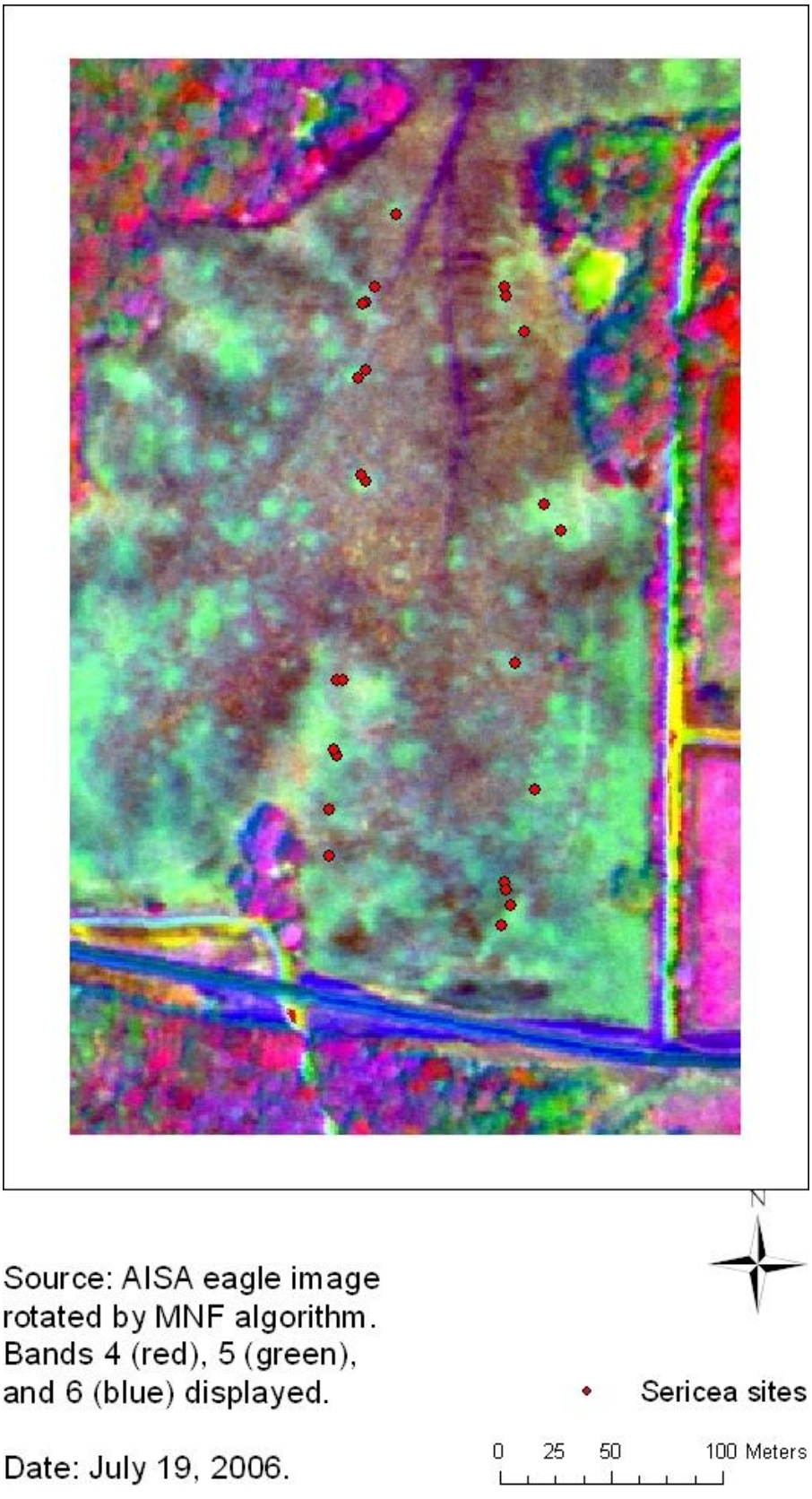

Figure 4-14: MNF image with components 4, 5, 6 displayed in RGB mode

4.1.3.2 MTMF mapping

Both of the MNF image and the MNF rotated endmember will be used as the input of MTMF mapping. The output has two sets of scores of MF and infeasibility corresponding to each pixel on the input image.

The two values were used in a 2-D scatter plot to interactively identifying sericea. In order to make the mapping result more visual friendly, the whole process was performed using the original AISA image as background (Figure 4-16). Figure 4-15 shows the scatter plot of MF score versus Infeasibility score of MNF rotated average sericea spectrum. The triangle shaped highlight area corresponds to the identified sericea pixels. The rationale for the triangle shape is the linear incremental effects of MF score versus Infeasibility score that when MF score is very low, it indicates the spectrum to be unlike sericea, the Infeasibility score will also be very low to ensure classifying it as sericea is unlikely to be wrong. These two criteria working together will ensure low omission and commission error in sericea classification.

Due to the subjectivity of this mapping method, a trial and error approach is taken. Multiple ROI specifications are tried on the 2-D scatter plot by changing the starting point and the slope of the ROI. Adjustments are made until the desired outcome is reached. The criteria for selecting the most appropriate ROI are: (1) all the visible sericea patches on the background image are covered, and (2) confusions with other class such as trees and grass are kept to minimum.

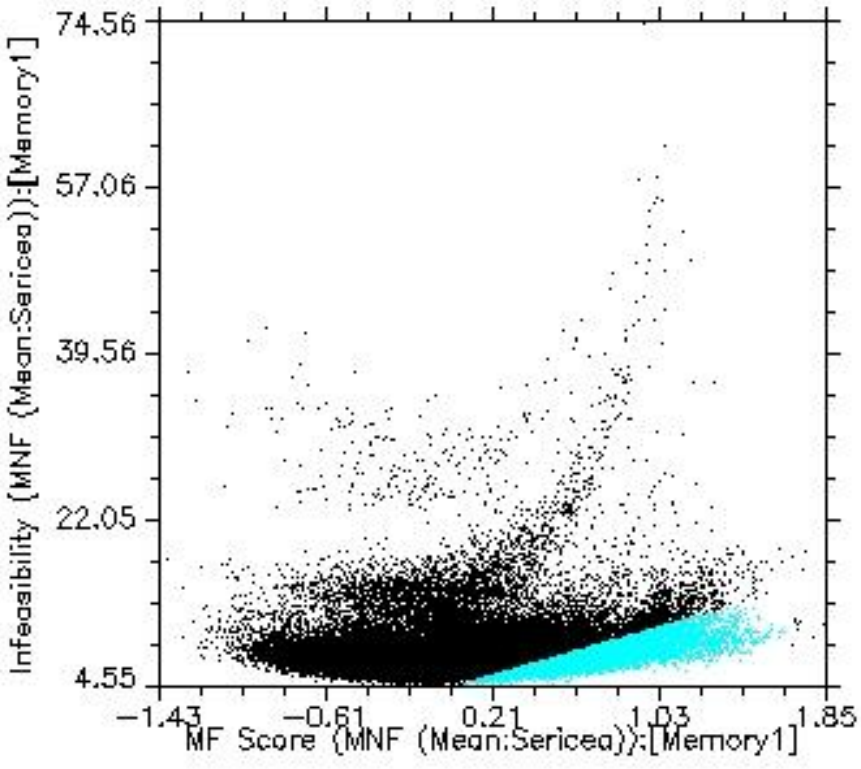

Figure 4-15: MTMF scatter plot (highlighted points have relatively high MF and low Infeasibility scores)

Figure 4-16 shows sericea patches highlighted in red which corresponds to the area highlighted in the scatter plot. This approach is so effective that almost all the visible sericea patches are picked up. More importantly, small patches of sericea are also picked up and some of the grass patches inside big sericea patches are excluded. Moreover, the confusion with trees is kept to minimum. Overall, this approach shows very promising results for identifying sericea from the hyperspectral image, at least from a visual interpretation. A sericea map is also extracted from this result and shown in Figure 4-17.

The sericea binary map is very noisy. So a majority filter was applied to the image and the output shown in Figure 4-18.

Figure 4-16: MTMF mapped sericea highlighted in red on top of the AISA image

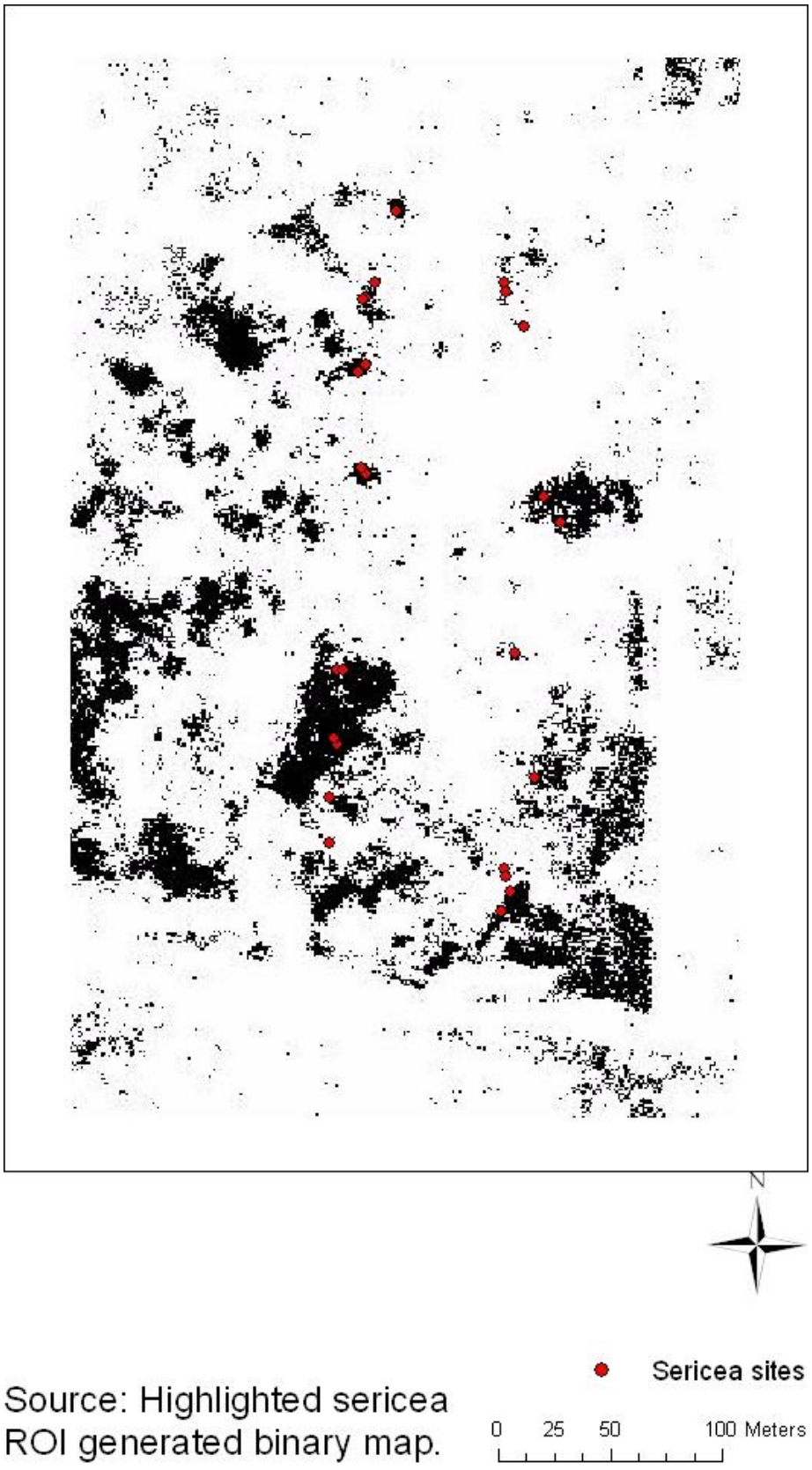

Figure 4-17: MTMF sericea map

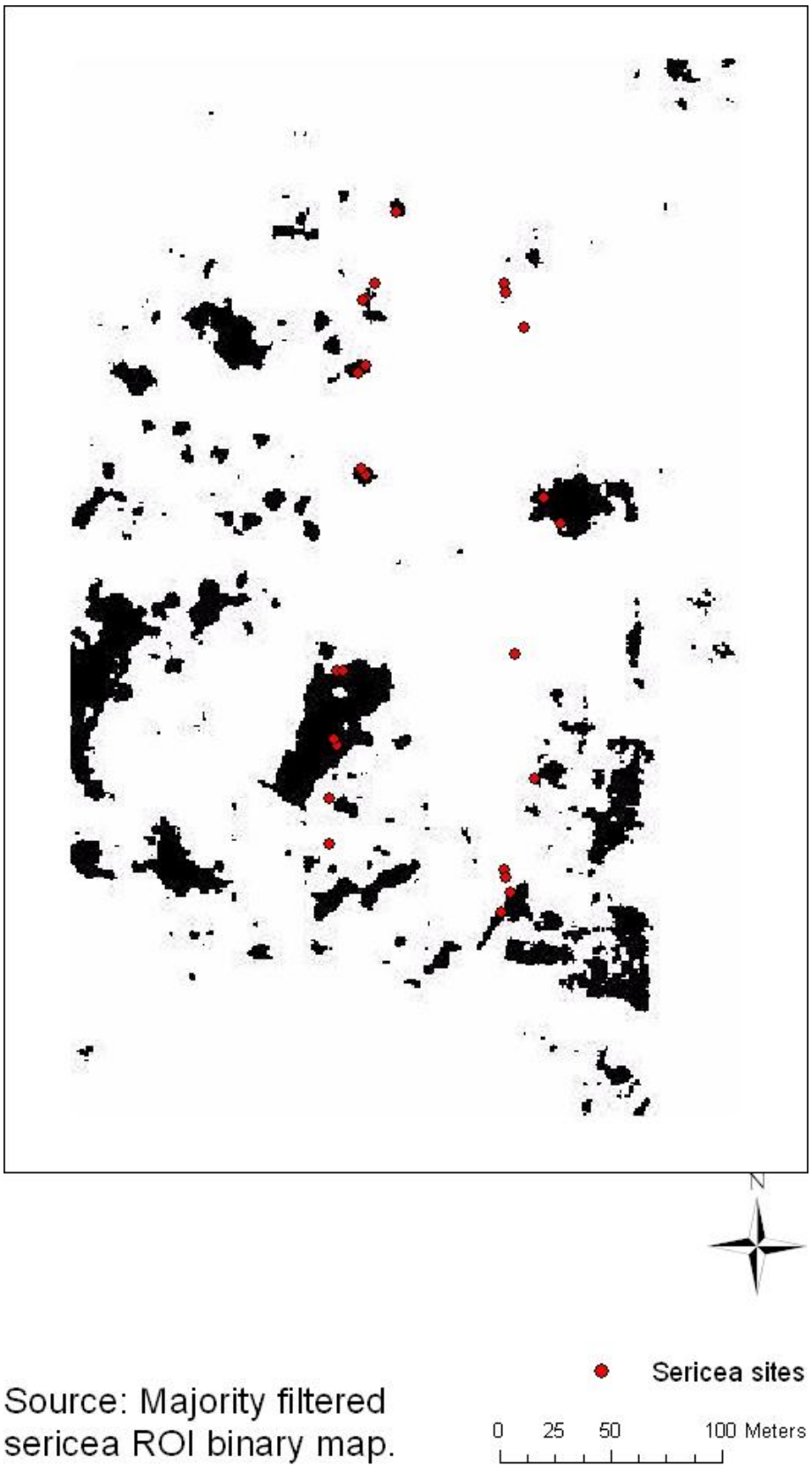

Figure 4-18: MTMF sericea map after majority filtering

4.2 Accuracy assessment

Visual inspection of the three classification results (Figures. 4-9, 4-11, and 4-18) shows similar sericea spatial distribution with differences in the shape coverage of the sericea patches. In the sericea map, the omission error is a major concern of classification accuracy due to the nature of sericea invasion; that if they are not killed once and for all they will come back again in a few years (Bové 2004 and Brush 2001). So the validation of sericea maps will only be performed on classified sericea to examine the producer's accuracy (omission error).

For the purpose of validation, an independent set of sericea ground sites were visited in April, 2007. These points were randomly scattered in the MTNF field (Fig 4-19). Accuracy assessment was performed based on the calculation of an error matrix. Two sources of information are compared in error matrix: (1) class value from the classified map, and (2) ground reference class value (which may have error). The relationship between these two sets of information is summarized in an error matrix or confusion matrix (Jensen 2005). Table 4-1 shows a sample error matrix which is used to assess the remote sensing classification accuracy of k classes. The columns represent the ground reference values and the rows are corresponding to the class values. The intersection of columns and rows summarize the number of sampled points assigned to a particular class. The total number examined is N. The diagonal of matrix summarizes points that were correctly classified. All the errors related to ground reference are summarized in the off-diagonal cells of the matrix. Each error is both an omission from the correct class and a commission to a wrong class. The column and row totals around the margin of the matrix

are used to compare errors of omission and commission. Omission error is calculated by each diagonal value divided by the corresponding column total and commission error is calculated by each diagonal value divided by the corresponding row total (Jensen 2005).

Table 4-1: Error matrix

Class	1	2	3	K	Row total
1	x_{11}	x_{12}	x_{13}	x_{1k}	X_{1+}
2	x_{21}	x_{22}	x_{23}	x_{2k}	X_{2+}
3	x_{31}	x_{32}	x_{33}	x_{3k}	X_{3+}
K	x_{k1}	x_{k2}	x_{k3}	x_{kk}	X_{k+}
Column total	X_{+1}	X_{+2}	X_{+3}	X_{+k}	N

A comparison of the overall accuracy results shows that the supervised MNF and MTMF joint approach performed the best with 75.00% overall classification accuracy, compared to 60.71% of the SAM approach, and 32.14% of the band ratio approach (Tables 4-2, 4-3, and 4-4).

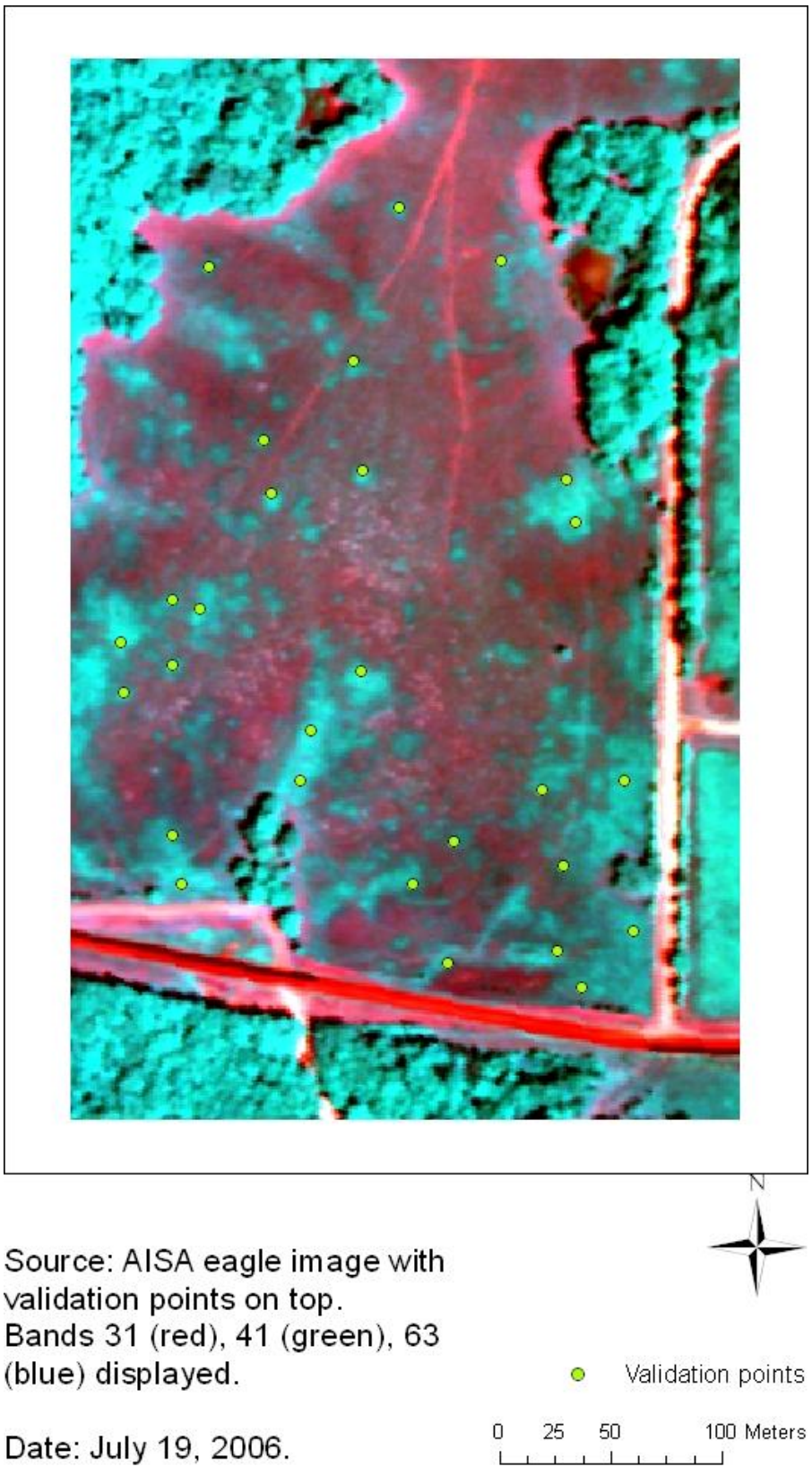

Figure 4-19: Validation sites overlaid on the AISA image

Table 4-2: Error matrix for classification on band ratio image

Classified Data	Unclassified	Sericea	Row Total
Unclassified	0	19	19
Sericea	0	9	9
Column Total	0	28	28

ACCURACY TOTALS

Class	Prod. Acc. (%)	Users Acc. (%)
Sericea	32.14%	100.00%

Overall Classification Accuracy = 32.14%

Table 4-3: Error matrix for classification on SAM image

Classified Data	Unclassified	Sericea	Row Total
Unclassified	0	11	11
Sericea	0	17	17
Column Total	0	28	28

ACCURACY TOTALS

Class	Prod. Acc. (%)	Users Acc. (%)
Sericea	60.71%	100.00%

Overall Classification Accuracy = 60.71%

Table 4-4: Error matrix for classification on MNF image

Classified Data	Unclassified	Sericea	Row Total
Unclassified	0	7	7
Sericea	0	21	21
Column Total	0	28	28

ACCURACY TOTALS

Class	Prod. Acc. (%)	Users Acc. (%)
Sericea	75.00%	100.00%

Overall Classification Accuracy = 75.00%

CHAPTER 5

DISCUSSION AND CONCLUSION

This study explores classification approaches using hyperspectral imaging to map invasive weeds in the grasslands of Missouri. Considering the ecological and economical impacts of invasive species, mapping their extent is a critical issue for many conservationists (Brush 2001, Bové 2004, Fishel 2002, Yates 2004). The contribution of this research is to map sericea in Missouri at a relatively high accuracy which cab in turn be used to limit the widespread application of herbicides. More importantly this research evaluated three different approaches of classification using airborne hyperspectral imagery.

5.1 Discussion

5.1.1 ASD derived endmember versus AISA derived endmember

Utilizing ASD field spectra measurement in endmember selection turned out to be a failure in this research. Although the spectra were preprocessed carefully with noise reduction, wavelength match, and resolution match to come up with a very high Pearson correlation with AISA spectra, the classification with the ground spectra was ineffective. The reasons may come from: (1) ASD measurement and AISA image acquisition were on different dates; (2) vegetation spectra are very similar (Lamb and Brown 2001) so that the spectra are sensitive to minor variation. A top-down approach was applied as an

alternative which utilized image spectra by extracting the Z-profile (ENVI 2002) with fieldwork acquired GPS coordinates. Then all sericea spectra were averaged to come up with the endmember in mapping out the sericea distribution in this research.

There are several considerations for extracting ASD-based endmembers in future applications. (1) field data and imagery should be acquired on the same date and under similar solar conditions; (2) atmospheric correction needs to be applied to image spectra and adjustment needs to be made to the corrected spectra if necessary, and (3) more endmembers in the same class could be selected to cover a huge variety of spectra, for example, endmembers of sericea at different density, color, height, and mixed cluster. It could be combined later to reach the maximum classification accuracy as was done in this research.

5.1.2 Geometric match between ground sites and image

In the process of endmember selection, the sericea patches recorded in May 2006 were found to be off the target of the image. It is probably due to the positional accuracy of the GPS unit used. The user's manual claimed to have a positional accuracy of 1~3 meters (Trimble 2005) based on single unit measurement. When plotted together with the image using more trustworthy points such as road intersections, the distance off seems to be around 5 pixels which correspond to 5 meters on the ground. The errors have a trend toward southeast. All ground sites are adjusted to northwest to counter the GPS measurement errors.

Accuracy assessment was performed using validation sites recorded in April, 2007. Only

28 sericea patches were identified (Figure 4-15), less than the 50 points per class suggested by Jensen (2000). The reason for the limited number of validation points is because the MTNF field was mowed in late fall of 2006. During the visitation this April, it is found that sericea is not recognizable in this early season. And the limited validation points were identified from dry stems of last year. With these limited validation sites, the accuracy was not high enough to conform to visual interpretation, especially with the MNF and MTMF approach that revealed very effective sericea patch mapping.

The GPS positioning error may also contribute to the low accuracy in the assessment. The mis-match between ground sites and the image affected small-size sericea patches the most. The positioning error could easily go beyond the diameter so that sericea site on the ground was mis-assigned as grass. In order to retain the objectivity of this research the validation points were not manually adjusted to match the visible sericea patches on a one by one basis, instead the same adjustment as applied to the field data was used. Provided with better GPS measurement such as Differential GPS (DGPS), the validation will show better results.

5.1.3 Mapping methods evaluation

5.1.3.1 Endmember selection

The rationale for band selection described in chapter 3 is as follows:

(1) In band ratio approach, only two bands were needed in the analysis, mostly one in red and the other in near-infrared based on past studies. In this study the two optimal bands in red and near-infrared were picked up;

(2) In SAM approach, band selection was based on the Hughes phenomenon and the fact

that less number of bands shortens the processing time although SAM with all bands is also tried; and

(3) The MNF-MTMF approach takes advantage of the MNF rotation on the available bands and information that is inherently in all bands. The MTMF algorithm produces two values for each pixel in an image: a Matched Filter value (MF) and an Infeasibility value. Pixels predicted as sericea were interactively selected based on a scatter plot of both MF scores and infeasibility scores. Pixels with high MF values and low infeasibility values were considered as sericea. The advantage of this approach is that the omission and commission error can be manually controlled and adjusted depending on the application. For example, in case pure sericea is desired, the classifier can set a very low infeasibility threshold to ensure low commission error. If small patches of sericea are also desired, both low MF threshold and low infeasibility threshold are set to reduce the omission errors in classification.

5.1.3.2 Mapping

Effective controlling of invasive species requires advanced knowledge of their spatial distribution and density (Underwood 2003). The MNF-MTMF joint approach on averaged sericea spectra has better result than band ratio and SAM methods. Performances of the three methods were summarized in this section.

Band ratio is only effective in picking up the outlines of sericea patches. Serious confusion is observed between different vegetation classes. If higher omission error is pursuit, commission error will increase rather rapidly as shown in (Figure 4-4, 4-5 and 4-6). The disadvantage of this approach is innate with the fact that it is using only a few

bands. Although this approach is the easiest one, it might not be feasible for application in mapping invasive species.

SAM is similar to MNF- MTMF joint approach, but in several aspects it is inferior to the latter: (1) the ability to pick up pixel size patches is limited, and (2) the ability to limit commission error while increase omission error is also limited as shown in Figure 4-8. The SAM approach is not optimal because it does not take advantage of the linear mixture theory (Boardman 1993) to reduce commission error while maintain low omission error. At a threshold angle of 0.03, the classification result has relatively smaller patch size than the ones of MNF-MTMF approach. Assigning a larger threshold angle dramatically increased the commission error. A lot of trees were then mis-classified as sericea. Both of these two approaches are using all available bands to be compared equally.

The MNF-MTMF joint approach has very clear patch delineation and very low confusion with other classes. It picks up small patches as shown in Figure 4-13 which are not identified in the other two approaches. Given more time to explore the MTMF scatter plot the mapping result could be further improved.

5.2 Conclusion

5.2.1 Filter for noise removal in ASD ground measurement

A spectral filtering technique is applied to ground-measured ASD spectra to reduce the noise from extensive water vapor absorption and system calibration errors. Two filters,

Mean filter and Savitsky Golay, are compared for their ability to remove noise in the data while maintain sharp spectral absorption/reflectance features. Savitsky Golay is a better than mean filter to reduce noise while preserving the spectral features of ground targets.

5.2.2 Optimal spectral bands

A Difference Ratio Ranking (DRR) is applied in this research to pick up optimal bands for sericea mapping. This approach itself is not questionable since it tries to capture the largest between-class variation in different bands. But for the purpose of vegetation differentiation, a few optimal bands may not be enough because different vegetation types may have similar spectral response (Lamb and Brown 2001). Exploring all bands in classification seems to be a better and more feasible option.

5.2.3 Mapping approaches

The band ratio approach is not an effective mapping approach because it results in high omission error when trying to keep low commission error. The SAM approach is very effective in picking up large sericea patches although small patches are often lost. The MNF-MTMF joint approach is most promising in identifying both large and small sericea patches while maintaining a relatively low commission error.

5.2.4 Major findings

The best way for endmember selection in classification of different vegetations is to use only one endmember to represent the target vegetation. In this research, the endmember is specified by averaging all the available spectra for sericea. The rationales to do so are: (1) average is the linear combination of all the spectra of sericea, it represents indirectly all

the possible sericea spectral signatures, (2) the average spectrum will have the least confusion with other classes since it has the farthest distance to other class spectra, and (3) the threshold can be set relatively larger until confusions happens between different vegetation classes.

A very interesting finding derived from this study is moderate spectral response of a specific class might be more effective for mapping purpose. It is believed that the most effective way of ground data collection is to use the ground object that has the strongest response, for example, in this research more measurements were contributed to high density, bright color and health sericea patches in the hope of locating more significant sericea signatures. But it was later found that these high density sericea spectra have the most confusion with trees. In view of the fact that this research uses the averaged sericea spectra as endmember, moderate sericea spectral response which is similar to averaged spectrum represented by lower density and greenness sericea patches may be more effective in identifying sericea with higher accuracy (low commission and omission error).

5.2.5 Future research

The next step for this study is to test the feasibility of these approaches toward a larger extent covering more habitat types and higher vegetative variation. More complicated approaches could also be examined. An exhaust of band combinations can be tried, and results can be plotted and compared. Then a threshold can be identified when the mapping accuracy does not increase with the increase of bands. This threshold can be

used to guide future mapping application.

More in depth research could be done toward a better understanding of vegetation spectra on multiple spatial and temporal dimensions. Ground spectra could be collected at different time, place and solar conditions to examine various factors that influence spectral signatures and later to be removed from spectra. A spectral library could be built to serve as reference in specific circumstances.

References

Adler-Golden, S. M., Matthew, M. W., Bernstein, L. S., Levine, R. Y., Berk, A., Richtsmeier, S. C., Acharya, P. K., Anderson, G. P., Felde, G., Gardner, J., Hike, M., Jeong, L. S., Pukall, B., Mello, J., Ratkowski, A., and Burke, H. -H. Atmospheric correction for shortwave spectral imagery based on MODTRAN4. *SPIE Proc. Imaging Spectrometry*, Vol. 3753: pp. 61-69, 1999.

Ashley, M. D., and J. Rea, Seasonal vegetation differences from ERTS imagery. *Photogrammetric Engineering and Remote Sensing*, Vol. 41: pp. 713-719, 1975.

Aspinall, R. J., W. A. Marcus, and J. W. Boardman, Considerations in collecting, processing, and analyzing high spatial resolution hyperspectral data for environmental investigations. *J Geograph. Syst.*, Vol. 4: pp.15-29, 2002.

ASD, Products-Software, Analytical Spectral Devices. Accessed: 03/01/07, http://www.asdi.com/, 2006.

Baret, F., G. Guyot, and D. J. Major, TSAVI: A vegetation index which minimizes soil brightness effects on LAI and APAR estimation. In: *Proceedings of the 12th Canadian Symposium on Remote Sensing*, IGRASS'89, July 10-14 1989 Vol. 3: pp. 1355-1358, 1989.

Barnes, E. M., Multispectral Remote Sensing and Site-Specific Agriculture: Example of Current Technology and Future Possibilities. *Proceedings of the 3rd International Conference on Precision Agriculture*, pp. 843-854, 1996.

Barnes, E. M., and M.G. Baker, Multispectral Data for Mapping Soil Texture: Possiblities and Limitations. *ASAE*, Vol. 16(6): pp. 731-741, 2000.

Berk, A. G. P. Anderson, L. S.Bernstein, P. K. Acharya, H. Dothe, M. W. Matthew, S. M. Adler-Golden, J. H. Chetwynd, Jr., S. C. Richtsmeier, B. Pukall, C. L. Allred, L. S. Jeong, and M. L. Hoke, MODTRAN4 Radiative Transfer Modeling for Atmospheric Correction. *SPIE Proceeding, Optical Spectroscopic Techniques and Instrumentation for Atmospheric and Space Research III*, Vol. 3756, 1999.

Bové, C., Missouri's Silent Thief. *Missouri Conservationist*. July, pp. 15-17, 2004.

Boardman, J. W., Automated spectral unmixing of AVIRIS data using convex geometry concepts: in Summaries. Fourth JPL Airborne Geoscience Workshop, *JPL Publication* 93-26, Vol. 1: pp. 11-14, 1993.

Brush, L., *Sericea* lespedeza. *Today's Farmer*, May, pp.14-15, 2001.

Campbell, J. B. Introduction to remote sensing (3rd Ed.). London: Taylor and Francis, 2002.

CALMIT, Program description, University of Nebraska-Lincoln. Accessed: 03/01/07, http://calmit.unl.edu/, 2006.

CHAMP, Program description, University of Nebraska-Lincoln. Accessed: 03/01/07, http://www.calmit.unl.edu/champ/index.php, 2006.

Chen, J. Y., and I. S. Reed, A detection algorithm for optical targets in clutter. *IEEE Trans. on Aerosp.*

Electron. Syst., Vol. AES-23, no. 1, 1987.

Dalal, R. C., R. J. Henry, Simultaneous determination of moisture, organic carbon and total nitrogen by near infrared reflectance spectrophotometry. *Soil Sci. Soc. Am. J.*, Vol. 50: pp.120-123, 1986.

Dennison, P. E., and D. A. Roberts, The effects of vegetation phenology on endmember selection and species mapping in southern California chaparral. *Remote Sensing of Environment*, Vol. 87: pp. 295-309, 2003.

Dudley, Dennis M., 2003 Effects of *Sericea* lespedeza residues on selected tallgrass prairie grasses. *Transaction of the Kansas Academy of Science*, Vol. 106: pp.166-170, 2003.

Elvidge, C.D., and R.J.P. Lyon, Influence of Rock-Soil Spectral Variation on Assessment of Green Biomass. *Remote Sensing of Environment*, Vol. 17: pp. 265-279, 1985.

Elvidge, C. D., and Zhikang Chen, Comparison of Broad-Band and Narrow-Band Red and Near-Infrared Vegetation Indices. *Remote Sensing of Environment*, Vol. 54: pp.38-48, 1995.

ENVI, The Environment for Visualizing Images (ENVI): ENVI Tutorials, Version 3.6, Research System Institute, USA, 2002.

ERDAS, Copyright 1991-2005 by Leica Geosystems Geospatial Imaging, LLC, 2005.

Fitzgerald, G.J., S.J. Maas, W.R. DeTar, Multispectral multitemporal remote sensing for spider mite detection in cotton. *Proceedings of Fifth International Conference on Precision Agriculture (CD)*, July 16_/19, 2000. Bloomington, MN, USA, 2000.

Fitzgerald, G. J., Spider Mite Detection and Canopy Component Mapping in Cotton Using Hyperspectral Imagery and Spectral Mixture Analysis. *Precision Agriculture*, Vol. 5: pp. 275-289, 2004.

Fishel, Fred, Noxious weeds of Missouri. *Integrated Pest Management*, 2002.

Gao, B.-C., K.H. Heidebrecht, and A. F. H. Goetz, Derivation of scaled surface reflectances from AVIRIS data. *Remote Sensing of Environment*, Vol. 44: pp. 165-178, 1993.

Gao, B.-C., C. Davis, and A. Goetz, A Review of Atmospheric Correction Techniques for Hyperspectral Remote Sensing of Land Surfaces and Ocean Color. *Geoscience and Remote Sensing Symposium*, pp. 1979-1981, 2006.

Gat, N., and H. Erives, Application of Low Altitude Aviris Imagery of Agricultural Fields In The San Joaquin Valley, Ca, To Precision Farming. *Precision Farming*, 1999.

Glenn, N. F., Hyperspectral data processing for repeat detection of small infestations of leafy spurge. *Remote Sensing of Environment*, Vol. 95: pp.399-412, 2005.

Goetz, A. F. H., et al., Imaging Spectrometry for Earth Remote Sensing. *Science*, Vol. 228, No. 4704, 1985.

Harsanyi, J. C., and C. I. Chang, Hyperspectral image classification and dimensionality reduction: An orthogonal subspace projection approach. *IEEE Trans. Geosci. and Remote Sens.*, Vol. 32: pp. 779-785, 1994.

Hughes, G. F., On the mean accuracy of statistical pattern recognizers. *IEEE Trans. Inf. Theory*, Vol. IT-14, no. 1, pp. 55-63, Jan. 1968.

Huete, A. R., R. D. Jackson, and D. F. Post, Spectral response of a plant canopy with different soil backgrounds. *Remote Sensing of Environment*, Vol. 17: pp. 37-53, 1985.

Huete, A. R., A Soil-Adjusted Vegetation Index (SAVI). *Remote Sensing of Environment*, Vol. 25: pp. 295-309, 1988.

Huang R., Band Selection Based on Feature Weighting for Classification of Hyperspectral Data. *IEEE Geoscience and Remote Sensing Letters*, Vol. 2, No. 2, Apr. 2005.

Ifarraguerri, A. Visual Method for Spectral Band Selection. *IEEE Geoscience and Remote Sensing Letters*, Vol. 1, No. 2, Apr. 2004.

Jensen, J. R., Remote Sensing of the Environment: An Earth Resource Perspective, Prentice Hall, Upper Saddle River, NJ, 2000.

Jensen, J. R., Introductory Digital Image Processing: A Remote Sensing Perspective, Prentice Hall, Upper Saddle River, NJ, 2005.

Jordan, C. F., Derivation of leaf-area index from quality of light on the forest floor. *Ecology*, Vol. 50(4): pp. 663-666, 1969.

Keshava N., Distance Metrics and Band Selection in Hyperspectral Processing With Application to Material Identifications and Spectral Libraries. *IEEE Geoscience and Remote Sensing Letters*, Vol. 42, No. 7, Jul. 2004.

Koger, Clifford H., 2003 Detecting Late-Season Weed Infestations in Soybean. *Weed Technology*, Vol. 17: pp. 696-704, 2003.

Kruse, F.A., Boardman, J.W., Lefkoff, A.B., Heidebrecht, K.B., Shapiro, A.T., Barloon, P.J., and Goetz, A.F.H. The Spectral Image Processing System (SIPS) – Interactive Visualization and Analysis of Imaging Spectrometer Data. *Remote Sensing of Environment*, Vol. 44: p.145-163, 1993.

Landgrebe, D. A., A perspective on the analysis of hyperspectral data. *Geoscience and Remote Sensing Symposium*, Vol. 3: pp. 1362-1364, 1993.

Lamb, D. W. and R. B. Brown, Remote-sensing and mapping of weeds in crops. *Jourinal of Agricultural Engineering Research*, Vol. 78(2): pp.117-125, 2001.

Lee, B. J., A. S. Woodyatt, and M. Berman, Enhancement of high spectral resolution remote sensing data by a noise-adjusted principal component transform. *IEEE Trans. Geosci. Remote Sensing*, Vol. 28, pp. 295–304, May 1990.

Mathur A., Exploiting Hyperspectral Hypertemporal Imagery with Feature Clustering for Invasive Species Detection. *IEEE International Geoscience and Remote Sensing Symposium*, pp. 828 – 831, 2006.

Qi, J., A. Chehbouni, A. R. Huete, Y. H. Kerr, and S. A sorooshian, modified soil adjusted vegetation index. *Remote Sensing of Environment*, Vol. 24: pp. 119-126, 1994.

Reid, D. B., E. Lithopoulos, and J, Hutton: Position and Orientation System for Direct Georeferencing (POS/DG). *Proceedings, Institute of Navigation 54th Annual Meeting, Denver, Colorado, USA*, June 1-3, pp. 445-449, 1998.

Shonk, J. L., et al. Spectroscopic sensing of soil organic matter content. Trans. *ASAE*, Vol. 34: pp.1978-1984, 1991.

Smith, L. A., United States Department of Agriculture-Agricultural Research Service research in application technology for pest management. *Pest Manag. Sci.*, Vol. 59: pp. 699-707, 2003.

Stocker, A. D., I. S. Reed, and X. Yu, Mulitdimensional signal processing for electrooptical target detection. *Proc. SPIE Int. Soc. Opt. Eng.*, vol. 1305, 1990.

Tanre, D., C. Deroo, P. Duhaut, M. Herman, J. J. Morcrette, J. Perbos, and P. Y. Deschamps, Description of a computer code to simulate the satellite signal in the solar spectrum: the 5S code. *Int. J. Remote Sensing*, Vol. 11: pp. 659–668, 1990.

Thorp, F. R., Tian, L. F., A Review on Remote Sensing of Weeds in Agriculture. *Precision Agriculture*, Vol. 5: pp. 477-508, 2004.

Tong, Q., B. Zhang, L. Zheng, Hyperspectral remote sensing technology and application in China. *Proc. of the 2nd CHRIS/Proba Workshop, ESA/ESRIN, Frascati, Italy* 28-30 2004.

Tucker, C. J., Red and photographic infrared linear combinations for monitoring vegetation. *Remote Sensing of Environment*, Vol. 8: pp. 127-150, 1979.

Ustin, S. L. et al., Hyperspectral Remote Sensing for Invasive Species Detection and Mapping. *Geosci. and Remote Sensing Symposium*, pp. 1658-1660. 2002.

Underwood, E. et al., Mapping nonnative plants using hyperspectral imagery. *Remote Sensing of Environment*, Vol. 86: pp. 150-161, 2003.

USDA plants database. Accessed 03/01/07, http://plants.usda.gov/java/profile?symbol=LECUS, 2007.

Varner, B.L., Gress, T.A., Copenhaver, K., Wax, L.M., Spragne, C.L., Tranel, P.J., 2000. Detection of cockleburs (XANTHIUM STRUMARIUM L.) in soybeans using hyperspectral imagery. *Proceedings of Fifth International Conference on Precision Agriculture (CD)*, July 16_/19, 2000, Bloomington, MN, USA.

Vincent, R.K., Multispectral Image Processing Methods. In Fundamentals of Geological and Environmental Remote Sensing. Prentice-Hall, Upper Saddle River, NJ, Chap. 5, pp. 100-149, 1997.

Vrindts, E., J. DE Baerdemaeker, and H. Ramon, Weed Detection Using Canopy Reflection. *Precision Agriculture*, Vol. 3: pp. 63-80, 2002.

Yates, Emily D., 2004 Recruitment of three non-native invasive plants into a fragmented forested forest in southern Illinois. *Forest Ecology and Management*, Vol. 190: pp. 119-130, 2004.

Yu, X., I. S. Reed, and A. D. Stocker, Comparative performance analysis of adaptive multispectral detectors, *IEEE Trans. on Signal Processing*, Vol. 41, no. 8, 1993.